AFWAL-TR-86-4038

*ADA 172623*

# ACETYLENE TERMINATED RESIN MECHANICAL CHARACTERIZATION

C. Leung

Rockwell International
Science Center
1049 Camino Dos Rios
Thousand Oaks, CA 91360

MAY 1986

Final report for the period
November 1980 through November 1985

MATERIALS LABORATORY
AIR FORCE WRIGHT AERONAUTICAL LABORATORIES
AIR FORCE SYSTEMS COMMAND
WRIGHT-PATTERSON AIR FORCE BASE, OHIO 45433

*20040224164*

CHARLES LEE, PROJECT ENGINEER
STRUCTURAL MATERIALS BRANCH
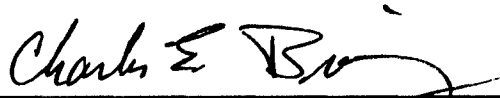
DR CHARLES E. BROWNING, CHIEF
STRUCTURAL MATERIALS BRANCH

FOR THE COMMANDER

MERRILL L. MINGES, DIRECTOR
NONMETALLIC MATERIALS DIVISION

# REPORT DOCUMENTATION PAGE

| 1a. REPORT SECURITY CLASSIFICATION | 1b. RESTRICTIVE MARKINGS |
|---|---|
| Unclassified | |

| 2a. SECURITY CLASSIFICATION AUTHORITY | 3. DISTRIBUTION/AVAILABILITY OF REPORT |
|---|---|
| | Approved for public release; distribution is unlimited. |
| 2b. DECLASSIFICATION/DOWNGRADING SCHEDULE | |

| 4. PERFORMING ORGANIZATION REPORT NUMBER(S) | 5. MONITORING ORGANIZATION REPORT NUMBER(S) |
|---|---|
| SC5292.181FR | AFWAL-TR-86-4038 |

| 6a. NAME OF PERFORMING ORGANIZATION | 6b. OFFICE SYMBOL (If applicable) | 7a. NAME OF MONITORING ORGANIZATION |
|---|---|---|
| Rockwell International Science Center | | Air Force Wright Aeronautical Laboratory Materials Laboratory (AFWAL/MLBC) |

| 6c. ADDRESS (City, State and ZIP Code) | 7b. ADDRESS (City, State and ZIP Code) |
|---|---|
| 1049 Camino Dos Rios Thousand Oaks, CA 91360 | AFWAL/MLBC WPAFB, OH 45433-6533 |

| 8a. NAME OF FUNDING/SPONSORING ORGANIZATION Air Force Wright Aeronautical Laboratories Materials Laboratory | 8b. OFFICE SYMBOL (If applicable) | 9. PROCUREMENT INSTRUMENT IDENTIFICATION NUMBER |
|---|---|---|
| | | Contract No. F33615-80-C-5142 |

| 8c. ADDRESS (City, State and ZIP Code) | 10. SOURCE OF FUNDING NOS. | | | |
|---|---|---|---|---|
| Wright-Patterson AFB Ohio 45433-6533 | PROGRAM ELEMENT NO. | PROJECT NO. | TASK NO. | WORK UNIT NO. |
| | 62102F | 2419 | 04 | 23 |

11. TITLE (Include Security Classification) ACETYLENE TERMINATED RESIN MECHANICAL CHARACTERIZATION (U)

12. PERSONAL AUTHOR(S)
Leung, C.

| 13a. TYPE OF REPORT | 13b. TIME COVERED | 14. DATE OF REPORT (Yr., Mo., Day) | 15. PAGE COUNT |
|---|---|---|---|
| Final Report | FROM 11/14/80 TO 11/29/85 | MAY 1986 | 67 |

16. SUPPLEMENTARY NOTATION

| 17 | COSATI CODES | | 18. SUBJECT TERMS (Continue on reverse if necessary and identify by block number) |
|---|---|---|---|
| FIELD | GROUP | SUB. GR. | ATS Resin, ATP resin, HR600P resin, cure kinetics, cure rheology, prepregging, composites, tertiary blends, fracture properties, cure states. |
| | | | |
| | | | |

19. ABSTRACT (Continue on reverse if necessary and identify by block number)

The physio-chemical and mechanical behavior of acetylene terminated polysulfone (ATS) were determined as a function of cure states. Given one pound of the resin (synthesized by Gulf under contract to AFWAL), cure kinetics, cure rheology and dynamic mechanical properties of the neat resin were measured. The following properties were also measured as a function of cure states as determined by residual exothermic or spectroscopic methods: thermophysical properties (glass transition temperatures, dilatation and free volume, surface energetics and moisture absorption/desorption kinetics); fracture energies; tensile properties; accelerated aging and computer-aided modelling. Prepregs of ATS were made with Celion 12K graphite fibers. Unidirectional and cross-ply laminates were fabricated and their mechanical properties were measured.

To improve the processibility and fracture properties of ATS, the resin was blended with HR600P and difunctional acetylene terminated phenylene oxide (ATP). Various blending ratios were investigated, and the thermophysical, rheological, dynamic mechanical and fracture properties of the blends were measured. The blends were found to improve the fracture properties of ATS without sacrificing the high temperature properties of ATS.

| 20. DISTRIBUTION/AVAILABILITY OF ABSTRACT | 21. ABSTRACT SECURITY CLASSIFICATION |
|---|---|
| UNCLASSIFIED/UNLIMITED ☒ SAME AS RPT. ☐ DTIC USERS ☐ | Unclassified |

| 22a. NAME OF RESPONSIBLE INDIVIDUAL | 22b. TELEPHONE NUMBER (Include Area Code) | 22c. OFFICE SYMBOL |
|---|---|---|
| Charles Y-C Lee | (513) 255-9075 | AFWAL/MLBC |

**DD FORM 1473, 83 APR** EDITION OF 1 JAN 73 IS OBSOLETE.

# FOREWORD

This final report covers the work performed under Contract F33615-80-C-5142, "Acetylene Terminated Resin Mechanical Characterization," during the period November 14, 1980 to November 29, 1985. This program was conducted under the technical direction of Dr. Charles Lee, Air Force Aeronautical Laboratories, Materials Laboratory, Wright-Patterson AFB, OH 45433-6533.

The program was carried out at the Science Center of Rockwell International Corporation, Thousand Oaks, CA 91360. Dr. Chuk Ling Leung was Program Manager and Principal Investigator. Mr. David Kaelble was Co-Investigator for the first 3 years of the program. Acknowledgement is given to Mr. Tony Liao for his timely technical support.

## TABLE OF CONTENTS

# LIST OF FIGURES

# LIST OF FIGURES

## LIST OF FIGURES

## LIST OF TABLES

# 1.0 INTRODUCTION AND APPROACH

Epoxy resins are the state-of-the-art polymers for graphite fiber reinforced composites as well as structural adhesives. They have achieved this status as the result of a unique combination of neat resin and composite properties as well as processing characteristics.

Unfortunately, in the past few years, the deficiencies of the epoxies have become apparent. This is particularly true when the polymer is exposed to hostile environments, such as high temperature and high humidity. Strength reduction as well as polymer structural degradation have occurred.

Recently, the Polymer Branch of the Air Force Wright Aeronautical Laboratories, Materials Laboratory has reported on a class of acetylene terminated polymers. Preliminary findings show that the AT polymers have significant potential as high temperature/high humidity replacement for epoxies. However, much is unknown about this new class of polymers and many properties remain to be determined. Additionally, data from an early study of the structure-property relationship of the new polymer will serve as a positive feedback for the tailoring of the polymeric structure to better suit the need in actual service environments.

The objective of this program is therefore to apply mechanical characterization methodology to one type of acetylene terminated polymers, i.e. acetylene terminated polysulfones (ATS). To achieve this goal, the polymer was provided by AFWAL/MLBP. Cure kinetics and rheometry were studied. Dynamic, fracture and mechanical properties of the polymers during different stages of cure were measured. Thermophysical properties of the fully cured polymers were studied. Accelerated aging of the polymer under hydrothermal exposure was studied. The chemical and mechanical behavior of the polymer at different cure states thus determined were compared with a polymer structure-properties computer model for predictive modelling. In addition to ATS, tertiary blends of ATS in two other AT polymers, i.e., 3-phenoxy 3'-ethynyl-diphenyl ether (ATP) and Hughes HR600P, were also studied. The objective of this phase of the program is to investigate the feasibility of improving the processibility and

1

fracture toughness of ATS by the other two components (ATP and HR600P) of the blend. The thermophysical, rheological, dynamic mechanical and fracture properties of the tertiary blends were measured as a function of ratios of the components.

## 2.0 BACKGROUND

Acetylene terminated polysulfone (ATS) was evaluated as matrix material for advanced composites. From a one-pound sample, neat resin characterization, thermophysical and fracture properties were measured as a function of different cure conditions (time and temperature). Basic composite properties were also obtained.

Neat resin characterization included differential scanning calorimetry, rheological and dynamic mechanical analysis during cure. Glass transition temperatures, dilatation free volume, surface energetics and moisture absorption/ desorption kinetics were measured. Fracture and tensile strengths of the neat resin were obtained as a function of temperature and aging conditions. The structure-property relationship of ATS was studied analytically by a computer-aided chemical model.

Prepregs were prepared from unsized Celion 12K graphite fibers using a laboratory single tow hot-melt prepregger. The "no-bag" autoclave technique was found to produce high quality void-free laminates. Laminates were cured according to an optimized cure cycle and tested for resin content, void, mechanical properties and fracture morphologies.

Tertiary blends of various ratios of ATS with 3-phenoxy-3'-ethynyl-diphenyl ether (ATP) and Hughes HR600P resin were investigated. The thermophysical, rheological, dynamic mechanical, fracture and tensile properties of neat resin samples of the blends were studied.

# 3.0 TECHNICAL DISCUSSION

## 3.1 Acetylene Terminated Polysulfone

Acetylene Terminated Polysulfone (ATS) was investigated during the first phase of the program. The uncured ATS monomer used in this study, the structure of which is shown in Fig. 1, was prepared under contract for the Air Force by Gulf Research and Development Co. The major component of this resin (about 75%) is 4,4'-bis(3-ethynylphenoxy) diphenyl-sulfone, with the remainder of the composition being primarily higher molecular weight oligomers (about 20%) and para-isomer (about 5%).[1]
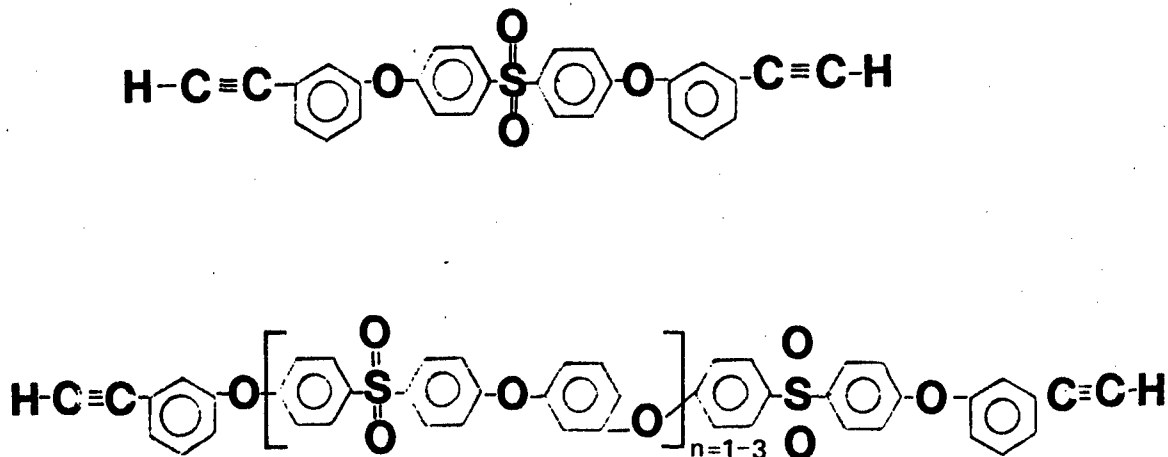




Fig. 1 Structure of acetylene terminated polysulfone (ATS).

## 3.1.1 Curing Kinetics of ATS

Differential scanning calorimetry of the received ATS samples were carried out at four scan rates: 5, 10, 20 and 40 C/min. The thermograms of dH/dt as a function of temperature at different thermal scan rates are shown in Fig. 2. It is seen that increased scan rate shifts the thermograms to higher temperature and also broadens the temperature range of curing. The graphical area beneath each curve identifies the heat of curing of the sample, as shown in Table 1. The data in the table show that while the heat of curing is relatively insensitive to scan rates, the temperature at which the curve maximizes increases as the thermal scan rate increases. This temperature maxima can be used to calculate the activation energy for polymerization via an Arrhenius-type rate equation,

SC85-34187
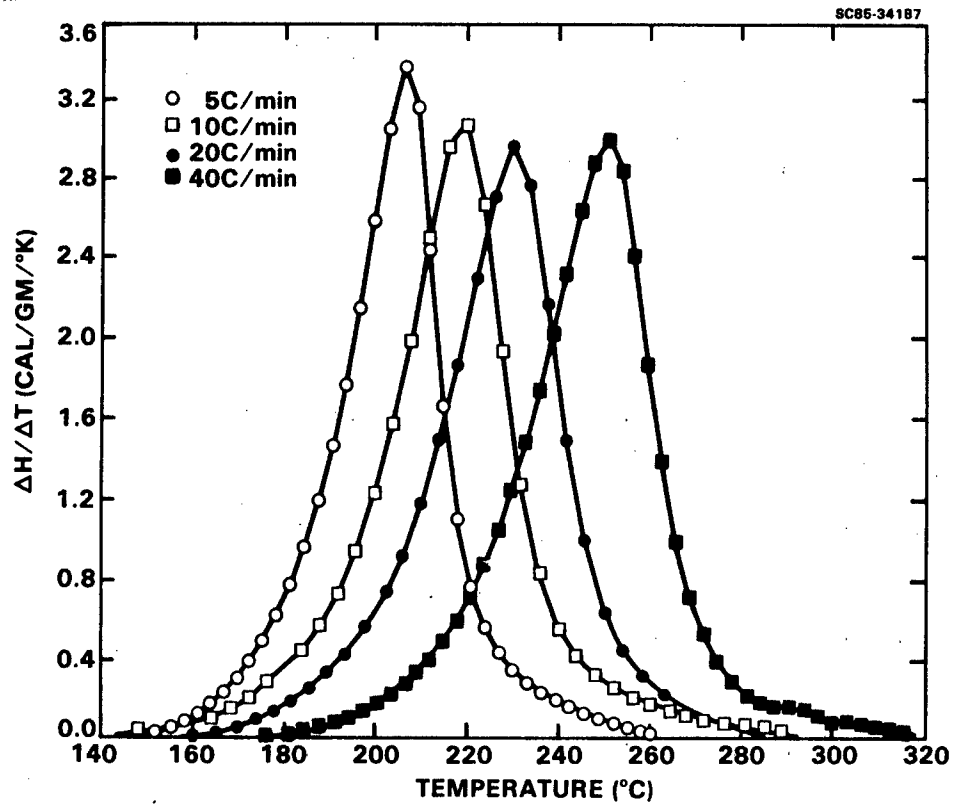


Fig. 2  Differential scanning calorimetry thermograms of ATS at
different scan rates.


Table 1

DSC Analysis of Cure of Acetylene
Terminated Polysulfone

| $\phi$ (K/min) | $\Delta H$ (cal/g) | T' (K) |
|---|---|---|
| 5 | 96.9 | 481 |
| 10 | 101.6 | 492 |
| 20 | 102.5 | 507 |
| 40 | 106.0 | 524 |

$$d \ln \phi/d(1/T') = -E/R -2T' \tag{1}$$

where $\phi$ is the scan rate, $T'$ is the temperature maxima, E is the energy of activation and R is the gas constant. Figure 3 shows that a plot of the data yields a straight line, the slope of which equal -E/R, giving an activation energy of 23.7 kcal/g for the polymerization of ATS. The heat of reaction (at 10°C/min) and activation energy are similar to those measured by Goldfarb,[2] who reported values of 115.9 cal/g and 21.3 kcal/mole, respectively.



SC85-34185
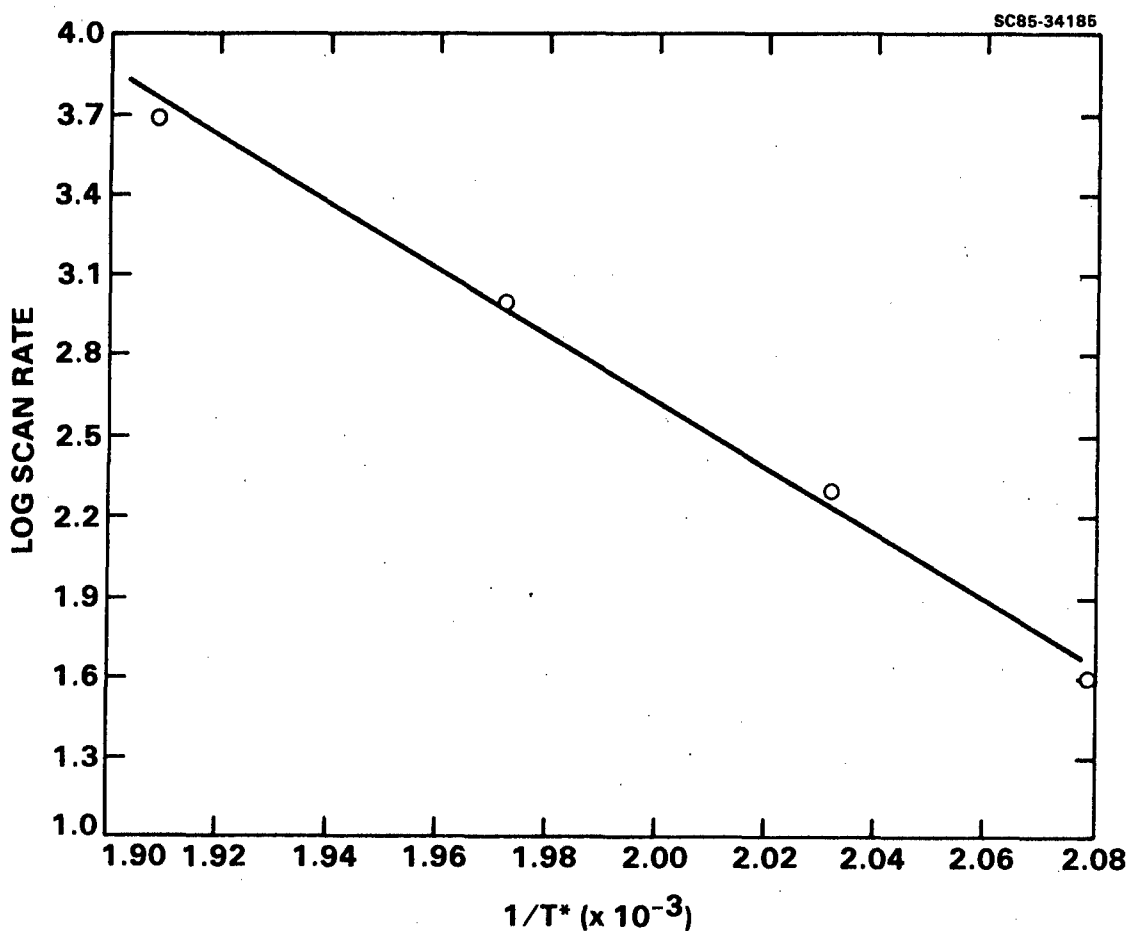
Fig. 3    Arrhenius plot of activation energy of polymerization
for ATS by DSC.

The DSC thermograms can also provide classical reaction/temperature window plots as shown in Fig. 4. The lines of the plot indicate the advancement toward cure completion (e.g. 5%, 50%, and 95% cured), providing convenient

6
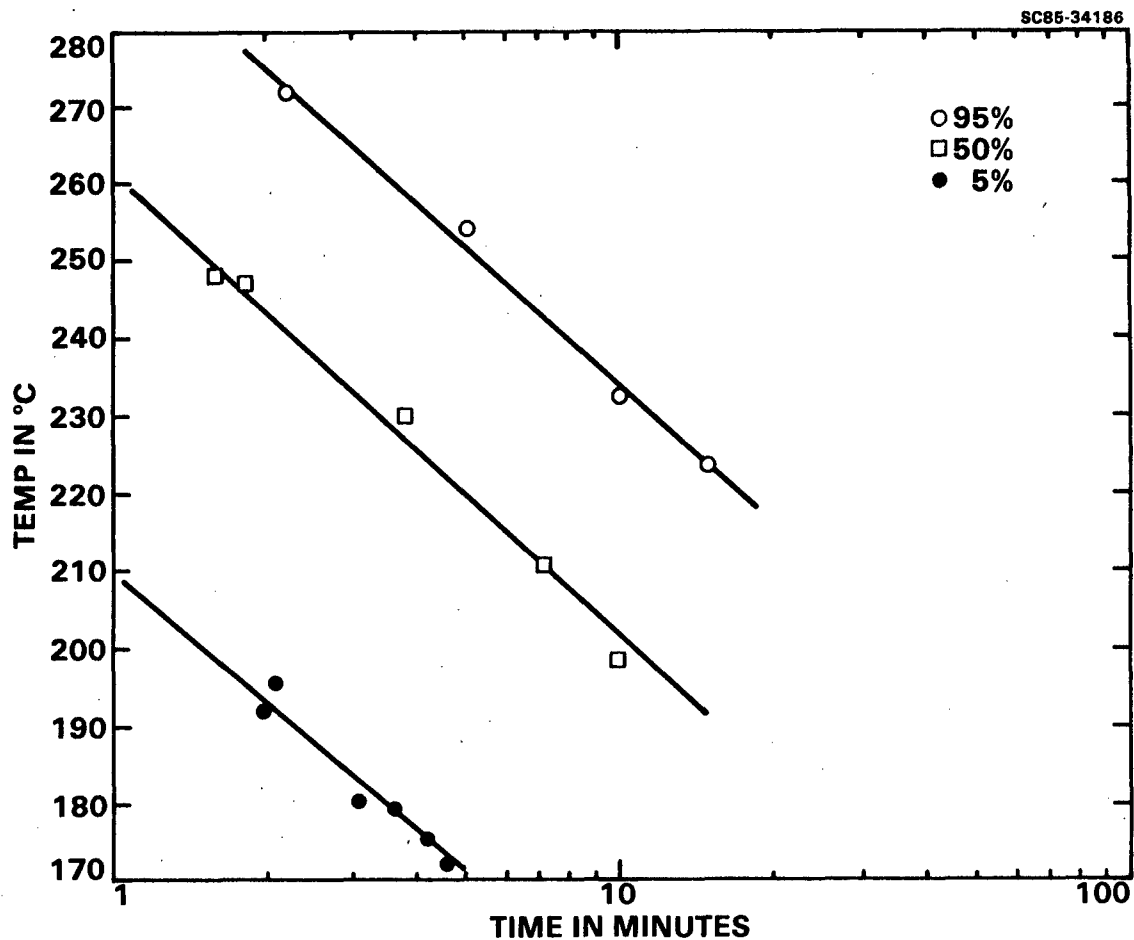
Fig. 4  Reaction/temperature window plots for ATS.

reference in the processing and fabrication of specimens.  As usual, the lines are extrapolated using first-order kinetic theory and consequently do not include consideration of other mechanisms such as molecular mobility of the curing resin.

### 3.1.2  Cure Rheology

The viscoelastic behavior of ATS resins was measured at scan rates of 2 and 5 C/min.  Specimens were placed between preheated parallel plates (50 mm) in a Rheometric Visco Elastic Tester and subjected to low frequency sinusoidal shearing at 10 rad/s, 10% strain.  The storage and loss moduli as well as the dynamic viscosity of the curing resin are shown in Figs. 5 and 6.  Due to the

7
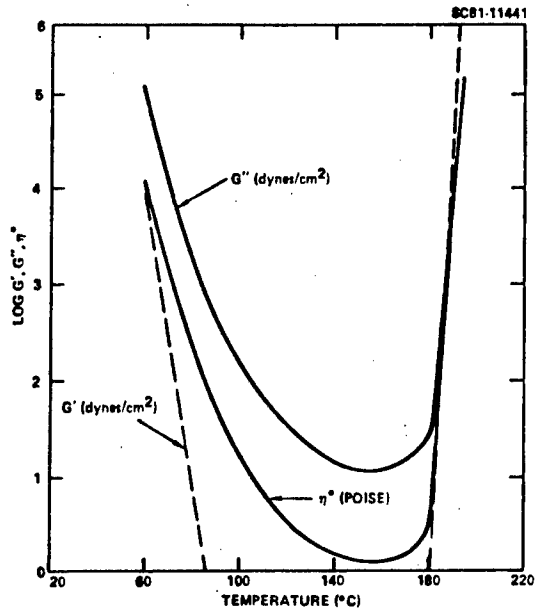
Fig. 5  Cure rheology of ATS at 2°C/min.
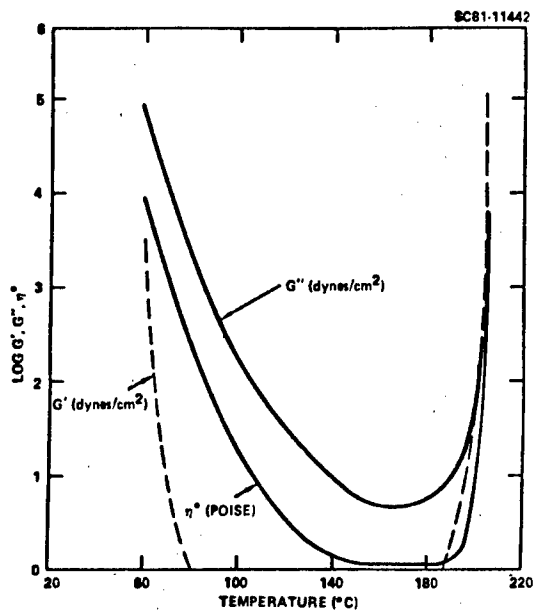


Fig. 6  Cure rheology of ATS at 5°C/min.

8

limited capacity of the load cell of the instrument, measurements were stopped prior to the peak of the curing thermograms. Nevertheless, it can be seen that the dynamic viscosities dropped rapidly with increasing temperature after introduction to the sample cavity, remaining quite low during the early stages of cure (140 to 180°C), then increased abruptly within a range of a few degrees, signifying the rapid formation of a high molecular weight structure or network.

The isothermal curing behavior of ATS was also studied. As shown in Figs. 7-9, it can be seen that the isothermal cure temperatures of 134 or 150°C, dynamic viscosities remained relatively low for about 15 to 25 minutes. At 178°C, the rise in viscosity is shown to be relatively rapid. The viscoelastically defined gelation times are tabulated in Table 2. The gel times of the ATS are much shorter than that of the purified all-meta ATS prepared by Fluorochem Inc., Irwindale, CA, reflecting perhaps residual initiators in the batch as prepared at Gulf.[3]
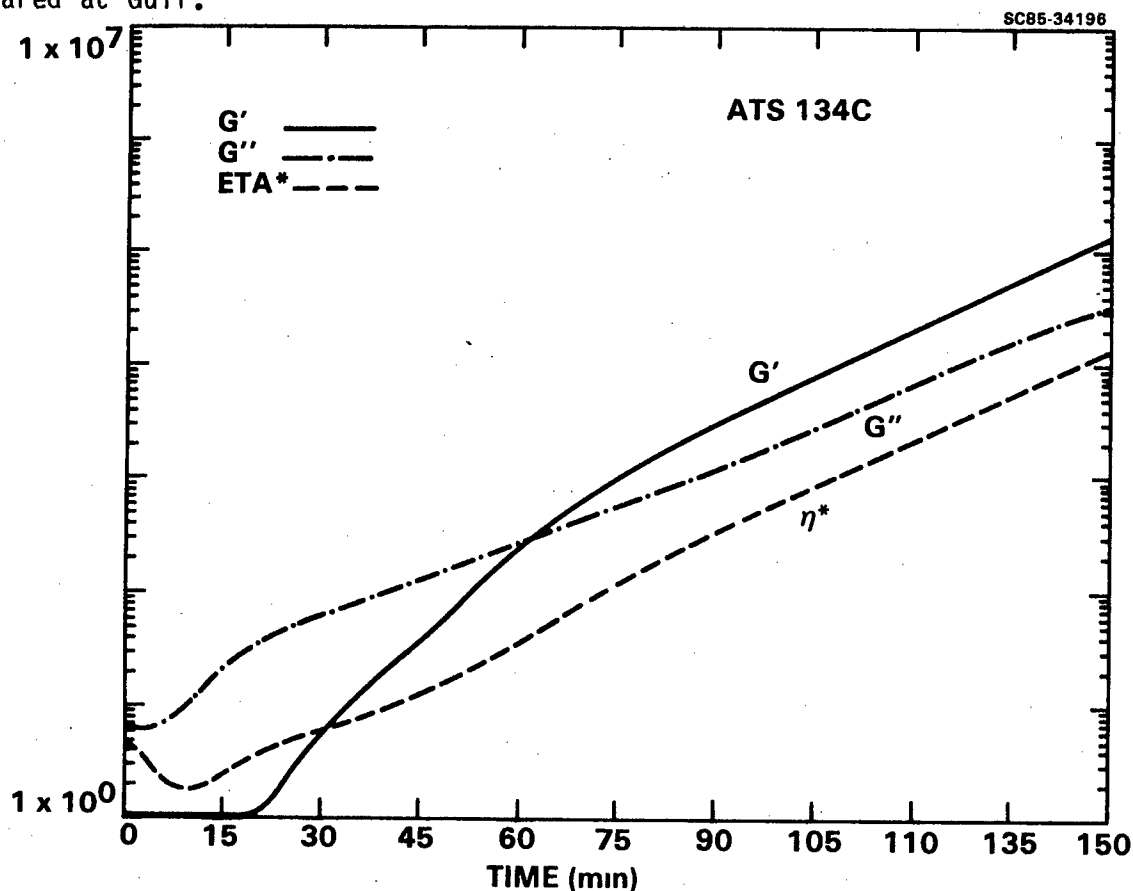


Fig. 7  Isothermal cure rheometry of ATS at 134°C.
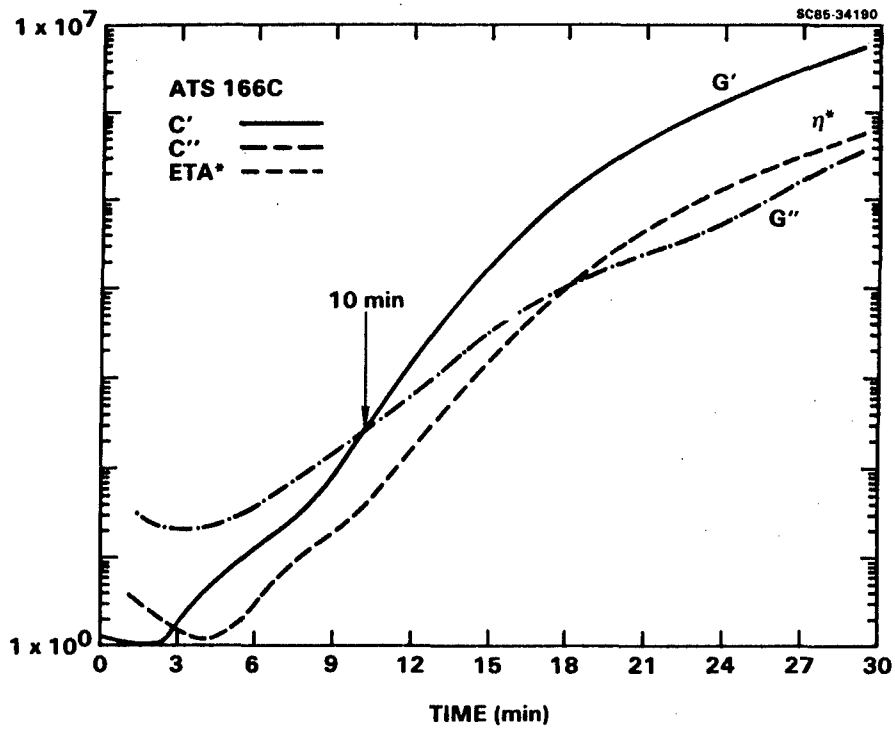
Fig. 8  Isothermal cure rheometry of ATS at 166°C.
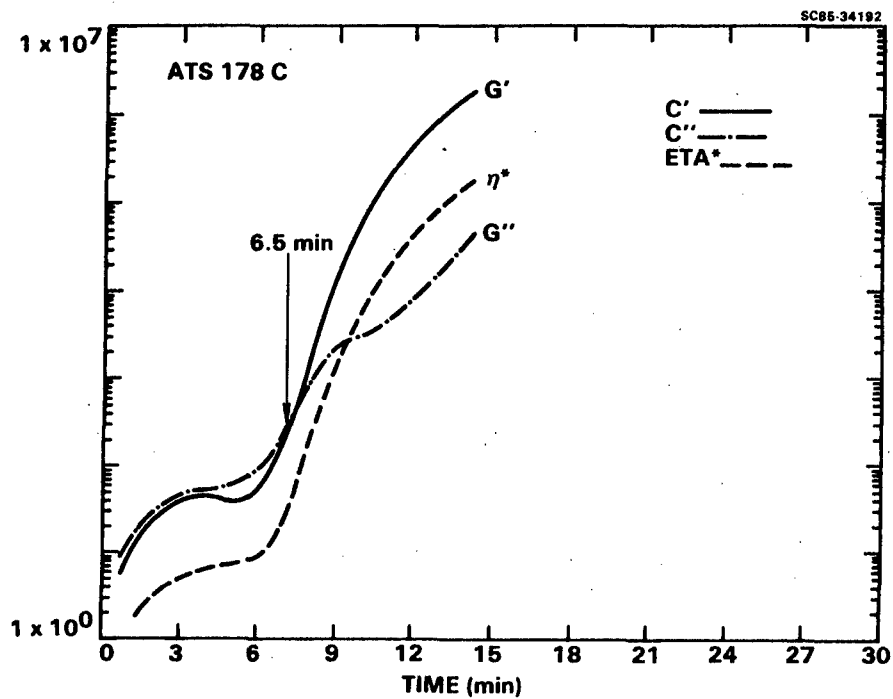


Fig. 9  Isothermal cure rheometry of ATS at 178°C.

10

## Table 2

### Dynamic Viscoelastic Analysis
### of Gelation for ATS

| Temperature (°C) | Gel Time (G' = G"), min | |
|:---:|:---:|:---:|
| | ATS (Gulf) | ATS (meta) |
| 134 | 60.2 | 250 (at 140°C) |
| 156 | 13.7 | 125 (at 150°C) |
| 166 | 10.5 | 70 (at 162°C) |
| 178 | 6.5 | 29 (at 177°C) |

The temperature dependence of gel time data is plotted according to an Arrhenius equation, as shown in Fig. 10, where an activation energy of 18.6 kcal/mole is obtained.
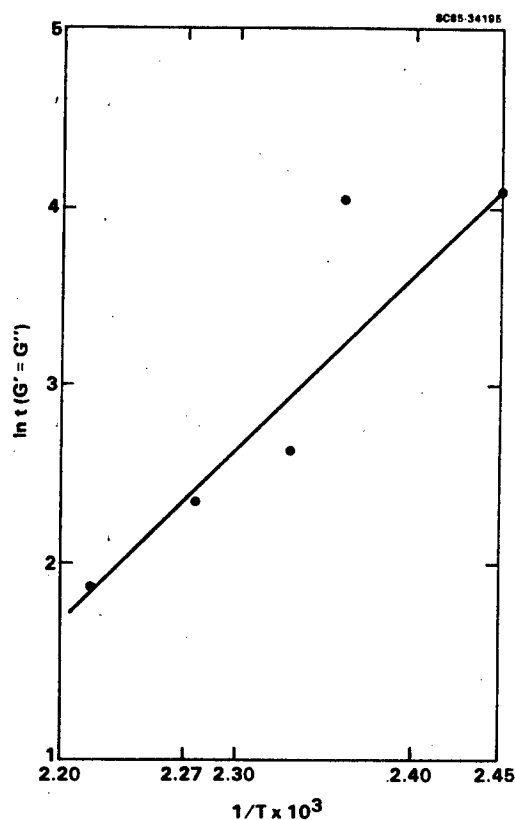


Fig. 10 Arrhenius plot of activation energy of polymerization for ATS by rheometry.

11

### 3.1.3 Dynamic Mechanical Properties of ATS During Cure

The measurement of a complete dynamic mechanical spectrum of ATS during cure was hampered by the upper limit of the Rheometrics transducer operating with the parallel-plate geometry. A rectangular torsional bar geometry was not feasible because of the lack of rigidity of the specimen: When the glass transition of the curing polymer was approached, the sample could not be clamped properly. One solution was to fabricate specimens in the form of rods with small diameters and carry out the experiment in a three-point flex mode in a rheovibron. The setup is shown schematically in Fig. 11. By precuring the specimen at 180°C for 10 min, thin specimen rods (about 1.8 mm in diam) with sufficient rigidity to be mounted onto the fixture were obtained and thermally scanned at a heat up rate of about 1.5°C/min.
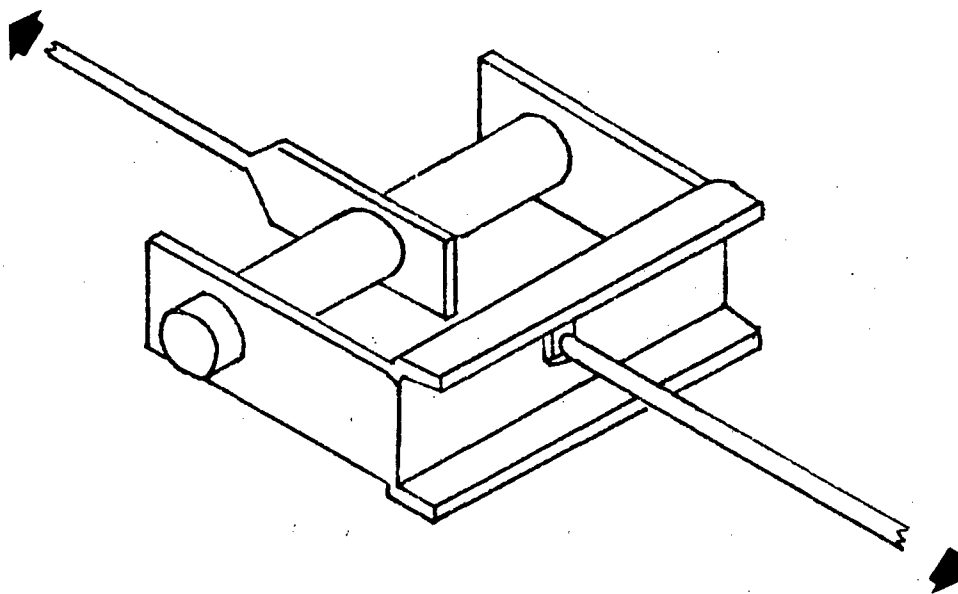
Fig. 11 Sample geometry for rheovibron.

Figures 12 and 13 show the storage moduli as well as the loss tangent of the polymer during the initial scan, rescan and post-cured scan. It can be seen that in the initial scan, at about 180°C, the polymer reached a flow state, as shown by the tremendously high loss tangent as well as a decrease in the storage modulus. At about 355°C, a second damping peak as well as a decrease in storage moduli occurred, caused by the glass-to-rubber transition of the polymer network. An immediate rescan of the polymer clearly showed the absence of the flow region and a better defined glass transition region for the crosslinked polymer. Postcuring the polymer at 300°C for several hours is seen to provide a progressively higher crosslink density for the network, as evidenced by the lowered peak height for the loss tangent together with a more gentle slope in the storage modulus-temperature transition. Thus, it appears that dynamic measurement of the neat polymer in the flexure mode via the Rheovibron provides a unique methodology for monitoring the cure of the polymer, in that the use of supporting braids or wires in the conventional torsional mode of excitation may introduce errors due to the polymer-support interface.
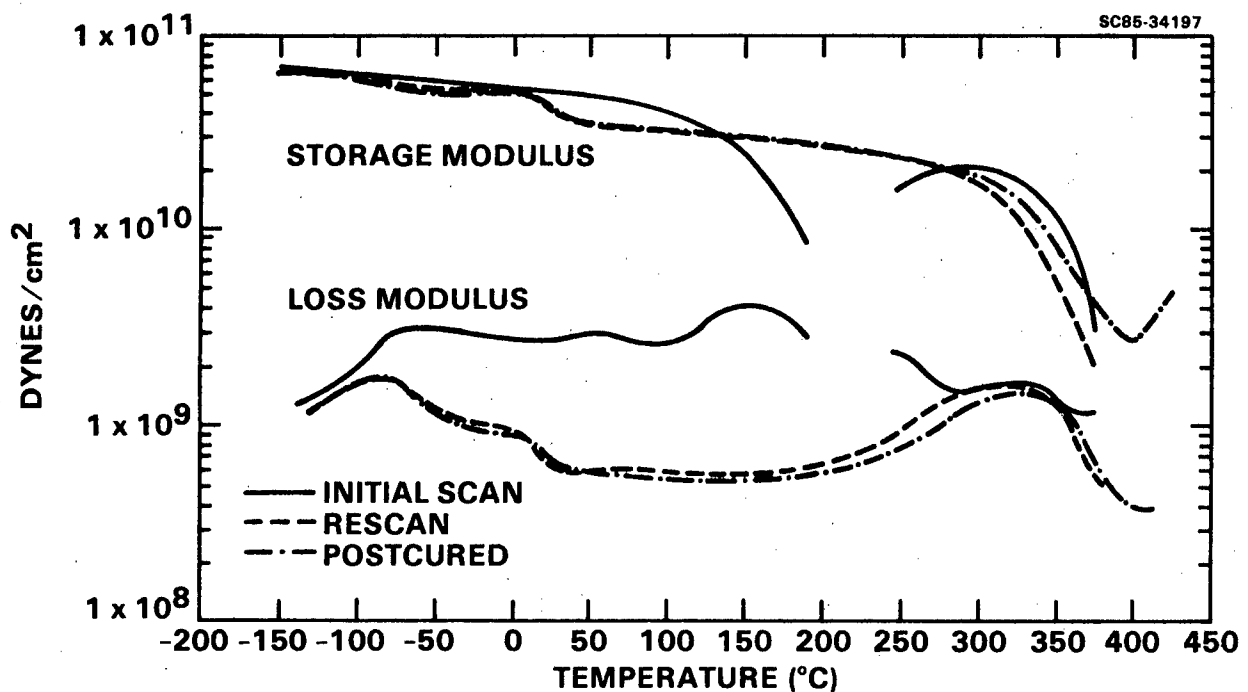


Fig. 12   Storage and loss moduli of ATS during cure.

13

**LOSS TANGENT OF ATS DURING CURE**
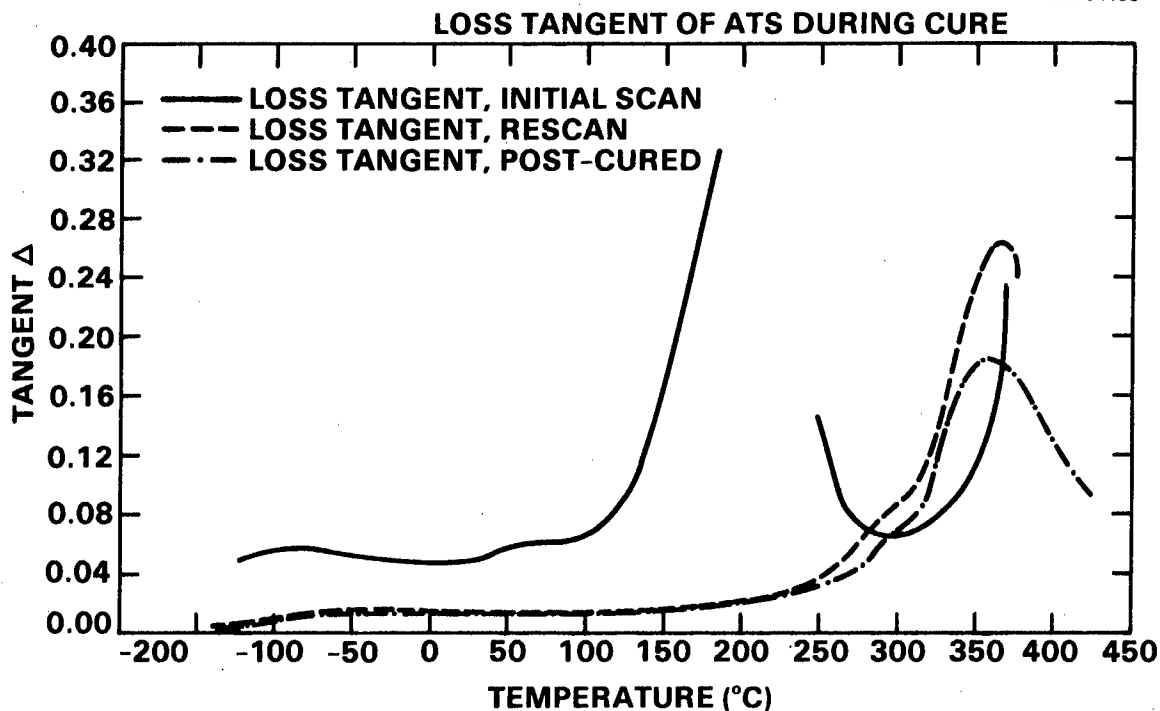


Fig. 13  Loss tangent of ATS during cure.

## 3.1.4    Degrees of Cure of ATS

### 3.1.4.1  Residual Exotherm

The curing exotherms of the ATS polymer as measured by differential scanning calorimetry (DSC) were used to establish the degrees of cure under various time/temperature conditions.  Initially, five temperatures were investigated:  130, 150, 180, 200 and 225°C.  Samples were prepared and cured isothermally to various times under nitrogen, cooled, and rescanned at 10°C/min. The degree of cure under the isothermal condition was calculated as

$$R = (\Delta H_T - \Delta H)/\Delta H_T \qquad (2)$$

where

$\Delta H_T$ = total heat of reaction (115 cal/g) for ATS and

$\Delta H$ = area under the rescanned exotherm.

14

It was found that at cure temperatures of 200°C and above, the reaction proceeded at such an accelerated pace that it would be very difficult to achieve thermal equilibrium throughout a relatively thick specimen, and would have resulted in a nonuniform state of cure within the sample. Accordingly, cure temperatures of 200 and 225°C were eliminated from the test matrix. The residual exotherm and degrees of cure data are tabulated in Table 3 and plotted logarithmically against 1/time in Figures 14 to 16.

Table 3

Residual Exotherms of Isothermally Precured ATS

| Temperature (°C) | Time (min) | H (cal/g) | Degree of Cure (%) |
|---|---|---|---|
| 130 | 90 | 108.7 | 5.5 |
| | 120 | 102.7 | 10.7 |
| | 150 | 99.4 | 13.4 |
| | 180 | 95.1 | 17.3 |
| | 300 | 77.6 | 32.5 |
| | 420 | 66.9 | 41.9 |
| | 549 | 51.4 | 54.9 |
| | 1230 | 27.8 | 75.9 |
| | 1440 | 21.2 | 81.6 |
| | 1815 | 17.2 | 85.0 |
| | 2670 | 15.8 | 86.2 |
| | 7200 | 11.7 | 89.8 |
| 150 | 20 | 108.4 | 5.8 |
| | 40 | 96.8 | 15.8 |
| | 51 | 88.2 | 23.3 |
| | 60 | 83.2 | 27.7 |
| | 70 | 75.8 | 34.1 |
| | 80 | 71.9 | 37.5 |
| | 460 | 13.3 | 88.5 |
| | 960 | 8.2 | 92.9 |
| 180 | 5 | 102.1 | 11.2 |
| | 10 | 76.3 | 33.7 |
| | 15 | 50.2 | 56.4 |
| | 20 | 39.7 | 65.5 |
| | 25 | 32.9 | 71.4 |
| | 30 | 20.4 | 82.3 |
| | 35 | 17.7 | 84.6 |
| | 40 | 12.5 | 89.1 |
| | 60 | 10.2 | 91.2 |
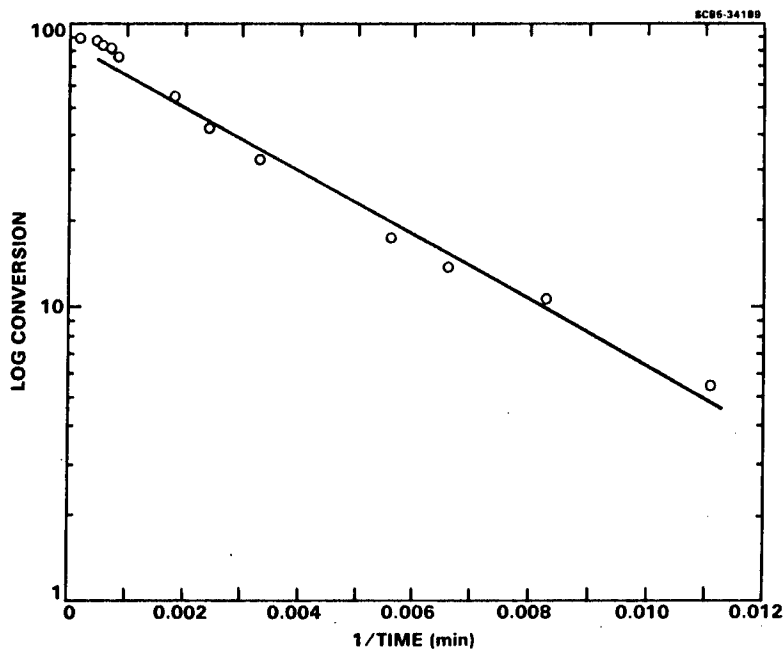
Fig. 14  Extent of reaction as a function of time at 130°C.
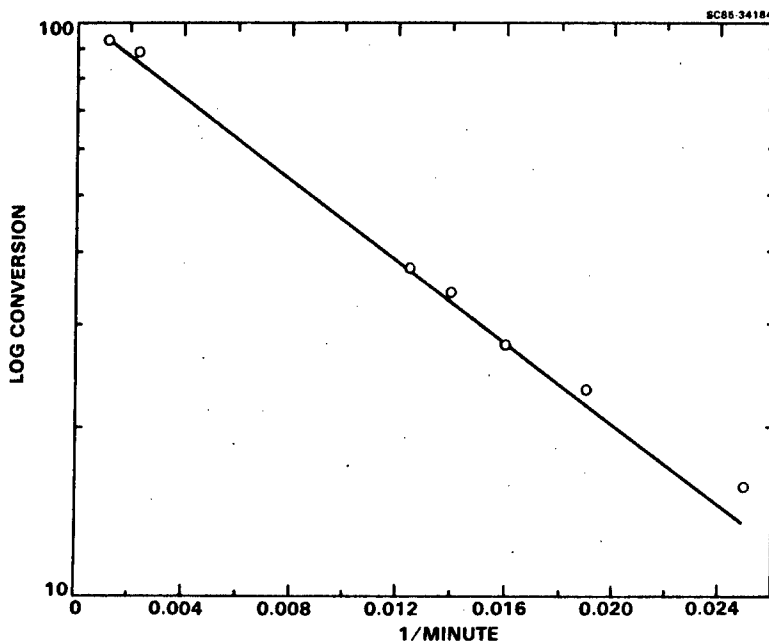


Fig. 15  Extent of reaction as a function of time at 150°C.
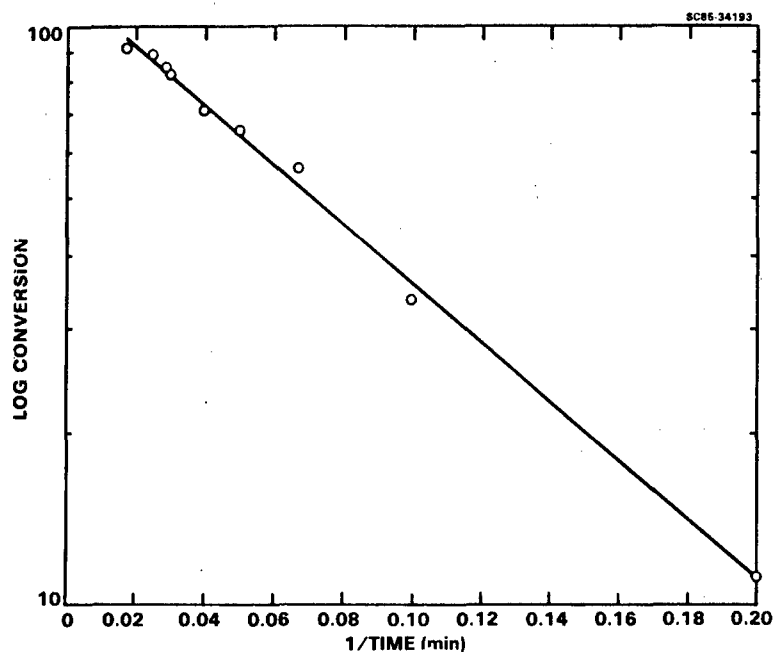
Fig. 16 Extent of reaction as a function of time at 180°C.

As shown in Figures 14 to 16, the semilog plots are linear at points below 90% cure, but these plots do not extrapolate to 100% cure even at extremely long cure times. This is a result of the thermal motion of the growing macromolecules being continuously hindered as the glass transition temperature of the system is being approached. Therefore the interpolation between degrees of cure and cure times which were used in this program was only made in the linear region of the plots.

## 3.1.4.2 Spectroscopic Parameters

In a parallel but separate program,[4] efforts were made to obtain spectral parameters of ATS that have undergone a variety of cure schedules and evaluate their potential as indicators of the network features characteristic of a given cure state. Fourier Transform Infrared Spectroscopy (FTIR), nuclear magnetic resonance (NMR) and Electron Spin Resonance (ESR) were the techniques investigated. The study found that while the degrees of cure as determined by

the residual exotherm are similar to those determined by FTIR at the early stages of cure, the residual exotherm method becomes less accurate as cure progressed. Using the area of the acetylenic absorption band at 3295 cm$^{-1}$ as an indicator, a comparison of the degrees of cure as determined by the thermal and spectroscopic methods are tabulated in Table 4.

Table 4

Comparison of Degrees of Cure Measured by Thermal and
Spectroscopic Methods

| Cure Conditions | | Degrees of Cure (%) | |
|---|---|---|---|
| Temperature (°C) | Time (min) | by DSC | by FTIR |
| 130 | 90 | 5.5 | 11.3 |
| | 185 | 17.5 | 20.4 |
| | 420 | 41.9 | 48.2 |
| | 1300 | 78.0 | 62.1 |
| | 1680 | 86.3 | 68.5 |
| 150 | 25 | 6.0 | 6.7 |
| | 51 | 23.0 | 11.1 |
| | 100 | 47.0 | 31.8 |
| | 200 | 70.0 | 58.0 |
| | 508 | 89.0 | 70.1 |
| | 600 | 91.0 | 73.2 |
| | 990 | 93.0 | 76.8 |
| 180 | 5 | 11.2 | 26.4 |
| | 10 | 33.7 | 33.9 |
| | 20 | 65.5 | 49.4 |
| | 30 | 82.3 | 62.1 |
| | 40 | 89.1 | 66.6 |
| | 60 | 91.2 | 71.4 |

Many rationales can be formulated to account for the discrepancies between the thermal and FTIR methods. Among them are: secondary curing reactions other than the acetylenic reactions measured by DSC, i.e., intramolecular cyclo addition (IMC); difficulty in establishing the correct baseline in residual exotherm measurements. One should therefore exercise considerable care in correlating reaction time with degree of cure in ATS polymers.

### 3.1.5    Thermophysical Properties of ATS

### 3.1.5.1  Glass Transition Temperature

Glass transition temperatures of the various cure states were measured using the penetration technique on the Thermal Mechanical Analyzer and are tabulated in Table 5.

Table 5

Glass Transition Temperatures of ATS Polymers

| Cure Temperature (°C) | % Cure (DSC) | Tg (C) |
|---|---|---|
| 130 | 40 | 77 |
|  | 60 | 88 |
|  | 80 | 135 |
|  | 90 | 164 |
|  | 100* | 350 |
| 150 | 40 | 86 |
|  | 60 | 120 |
|  | 80 | 132 |
|  | 93 | 159 |
|  | 100* | 348 |
| 180 | 60 | 128 |
|  | 80 | 152 |
|  | 90 | 153 |
|  | 100* | 350 |

*Postcured at 300°C for 2 h.

The data, when plotted in Figure 17, show that while the glass transition temperatures increase, as expected, as cure time increases, there is not a dramatic difference between the three cure temperatures, even at 90% cure (as measured by DSC).  However, there is a dramatic increase in Tg that accompanied the completion of the remaining 10% cure (by heating at 300°C for 2 h).  This implies a rapid transformation of the network structures within each cure state to that of a much higher crosslink density.  Presumably this can be accomplished by either the consolidation of clusters of lightly crosslinked species or the
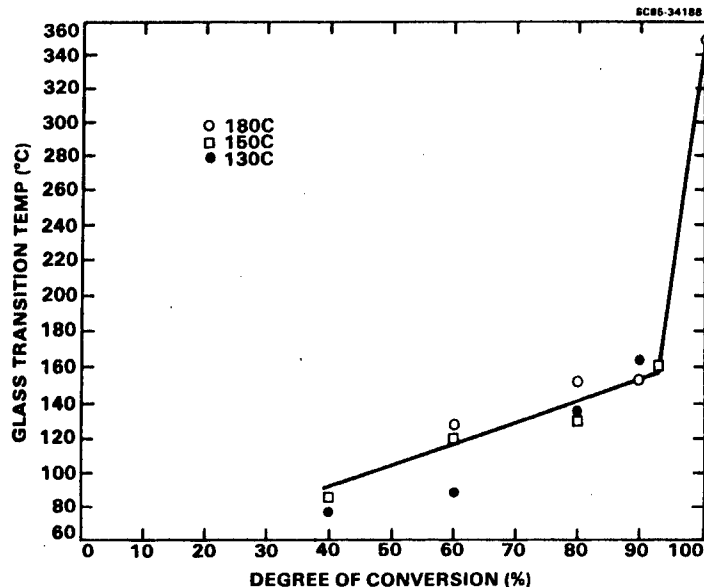
Fig. 17  Glass transition temperatures of ATS as a function of
cure time at various cure temperatures.

simultaneous activation of most of the crosslinkable sites within the specimen,
most probably the residual double bonds remaining after the reaction of the
acetylenic end groups.

### 3.1.5.2  Dilatation Characteristics and Free Volume

The coefficients of thermal expansion of ATS polymers at various cure
states as well as the fully cured specimens were measured by TMA.  Coefficients
of thermal expansion in the glassy and rubbery regions were calculated by draw-
ing a tangent to the glassy and rubbery regions of the TMA traces, respectively.
The linear coefficients of thermal expansion for the various cure states are
tabulated in Table 6.

It is interesting to note that the expansion coefficients in the glassy
regions decrease as the degree of conversion increase.  This seems to agree with
the hypothesis that as conversion increases, consolidation of random molecules
into a more compact network structure would decrease the normal thermal

## Table 6

### Linear Coefficients of Thermal Expansion of ATS Polymers at the Glassy and Rubbery Regions

| Cure Temperature (°C) | % Cure (by DSC) | $\alpha_g(\times 10^{-5}/°C)$ | $\alpha_r(\times 10^{-4}/°C)$ |
|---|---|---|---|
| 130 | 40 | 4.45 | |
| | 60 | 4.35 | |
| | 80 | 4.05 | |
| | 90 | 3.96 | |
| | 100* | 3.95 | 20.4 |
| 150 | 40 | 4.35 | |
| | 60 | 4.20 | |
| | 80 | 4.18 | |
| | 93 | 4.17 | |
| | 100* | 4.09 | 19.5 |
| 180 | 60 | 4.26 | |
| | 80 | 4.23 | |
| | 90 | 4.19 | |
| | 100* | 3.93 | 20.4 |

*Postcured at 300°C for 2 h.

expansive processes. Boyer has indicated that there is a pronounced relationship between the volume expansivities, $\Delta\alpha$, and the structure of the polymer. Simha and Boyer have suggested the following relationships to arrive at the fractional free volume below the glass transition:

$$V_f/V_g = \Delta\alpha Tg \tag{3}$$

where

$V_f$ = the frozen-in excess volume in the glassy state

$V_g$ = total volume at Tg, and

= volume expansion of free volume close to the Tg

$\Delta\alpha = \alpha_r - \alpha_g$, the coefficients of volume expansion at the rubbery and glassy regions, respectively.

Using Eq. (3), the fractional free volume of the fully cured ATS polymer is equal to $(2.01 - 0.399) \times 10^{-4} \times 623 = 0.1004$. A mean value of the fractional free volume obtained by Simha and Boyer is 0.113, a figure obtained for polymers with a molecular weight greater than 10,000 and relatively free from motions attributable to side groups. Thus the fractional free volume of 0.1004 obtained for ATS polymer indicates either a high molecular weight, or a less flexible chain structure, or both, than the typical polymers investigated by Simha and Boyer. It has been shown[5] that one crosslink reduces the occupied volume of a typical polymer by $144\text{\AA}^3$ - one half of the occupied volume of a single monomer unit - and reduces the free volume by $34\text{\AA}^3$ - three to four times the free volume associated with a single monomer unit. Based on the structural configuration of the ATS monomer, it is perhaps prudent to suggest that high crosslink density is the primary cause, and the chain stiffness as a secondary cause, for the low free volume of ATS polymer.

### 3.1.5.3  Surface Energetics

The surface energetics of ATS polymers were measured by measuring the contact angles of the polymer using the Rame-Hart goniometer. Sessile drops of 0.005 ml of 10 reference liquids were used. Using the linear least square fit, the polar and dispersive components of the surface energy of the polymer were calculated. Table 7 shows the surface energy properties of the ATS polymer as a function of cure conditions.

The data in Table 7 show that the surface energy properties of fully cured ATS are very similar to those of epoxy resins. One interesting phenomenon is the comparatively low polar part of the surface tension at low cure conversions. It appears that at low conversions, the polar ether and sulfone entities in the ATS molecule are somehow hidden within the macromolecules, and are exposed only at high conversions and when fully cured.

The surface energies of a polymer are also important parameters in the proper selection of fibers in the fabrication of reinforced composites. Since the wetting of ATS onto the fibers occurs when the polymer is in the molten

Table 7

Surface Energy Properties of ATS Polymer

| Cure Temperature (°C) | % Cure by DSC | $\gamma^d$ (mJ/m$^2$) | $\gamma^p$ (mJ/m$^2$) | $\gamma$ (mJ/m$^2$) |
|---|---|---|---|---|
| 130 | 40 | 36.4 | 9.2 | 45.6 |
| | 60 | 38.8 | 10.8 | 49.6 |
| | 80 | 32.4 | 18.6 | 51.0 |
| | 90 | 33.3 | 14.6 | 47.9 |
| | 100* | 29.6 | 21.1 | 50.7 |
| 150 | 40 | 34.0 | 9.8 | 43.9 |
| | 60 | 32.9 | 18.0 | 50.9 |
| | 80 | 34.3 | 15.3 | 49.6 |
| | 93 | 35.2 | 11.2 | 46.5 |
| | 100* | 33.4 | 17.5 | 50.9 |
| 180 | 60 | 38.0 | 10.3 | 48.3 |
| | 80 | 37.8 | 10.5 | 48.3 |
| | 90 | 32.3 | 20.1 | 52.3 |
| | 100* | 34.5 | 18.5 | 53.0 |
| Narmco 5208 | | 33.3 | 17.0 | 50.0 |

*Postcured at 300°C for 2 h.

state, it is thought that the surface energies of ATS melt, rather than of the solid, would provide more realistic parameters in the choice of graphite fibers.

To measure the surface energetics of ATS melt, the following steps were taken:

1. The contact angles of the liquid, i.e. ATS melt, on four standard solids whose a and B value are known: Teflon, glass, nylon 66 and kapton were measured.

2. The surface tension of the liquid (ATS melt) was measured at 140°C by the Wilhelmy plate method, using a platinum wire with a radius of 0.05 cm.

3. Contact angles of the liquid (ATS melt) were then measured on the four standard solids which were heated to 140°C.

The surface tension of the ATS at 140°C was found to be 31.8 dynes/cm. Contact angle measurements yielded $\beta(L)$ and $\alpha(L)$ values of 2.28 and 6.0 dyne/cm, respectively. Taking the squares, $\gamma_p$ for ATS melt equals 5.2 with $\gamma_d$ equals 36.4. The total surface tension of ATS melt at 140°C is therefore 41.6 dyne/cm. The result indicates that fibers with a total surface tension higher than 41.6 dyne/cm would be expected to provide favorable adhesion for the ATS resin during prepregging. Celion 12K unsized, having a total surface tension of 51.8 dyne/cm, as compared to that of 43.9 dyne/cm for AS4, appears to be a good candidate and was chosen for the fabrication of prepregs.

### 3.1.5.4  Moisture Absorption/Desorption Kinetics

Moisture absorption was measured by immersing a thin specimen in a thermostatted water bath and measuring the weight gain as a function of time. The data were then plotted, with $(time)^{1/2}$ on the abscissa and percent weight gain on the ordinate. The initial slope, S, of such a plot was used to calculate the diffusion coefficient, D', as follows:[6]

$$D' = S^2 h^2 \pi/16 \tag{4}$$

where h = specimen thickness. However, as the edges of the specimen were not sealed, a correction for edge effect was used:

$$D' = D [1+ h/L + h/W]^2 \tag{5}$$

where          D = corrected diffusion coefficient
          h, L, W = specimen thickness, length and width, respectively.

Moisture desorption kinetics was determined on the saturated samples by the DuPont Moisture Evolution Analyzer at the same temperatures as the absorption experiments. The desorption rates were measured and the moisture desorption coefficients were calculated, again using Eqs. (4) and (5).

Moisture absorption and desorption experiments were conducted at temperatures of 25, 50 and 75°C. The activation energies of absorption and desorption, $E_a$ and $E_d$, respectively, as well as the pre-exponential terms, were calculated by an Arrhenius-type relationship:

$$D = D_0 \exp (-E/RT). \tag{6}$$

On taking logarithms, Eq. (6) becomes

$$\log D = \log D_0 - (E/R) \, 1/T \tag{7}$$

where

$D$ = diffusion coefficient

$D_0$ = pre-exponential constant, and

$T$ = temperature.

Diffusion coefficients for moisture absorption and desorption for ATS polymer at various temperatures are tabulated in Appendix A. Narmco 5208 epoxy was included for comparison, as moisture effect on the material has been widely reported in the literature. Activation energies and pre-exponential factors for absorption and desorption for the fully cured ATS polymers were calculated using Eqs. (6) and (7), as shown in Table 8.

From the hole theory of diffusion, the rate of diffusion will depend on (a) the number and size distribution of pre-existing holes, and (b) the ease of hole formation. The former will depend on the ease and degree of packing of the

Table 8

Activation Energies and Pre-exponential Factors of Moisture
Absorption/Desorption for ATS Polymer

| Cure Temperature (°C) | Absorption | | Desorption | |
|---|---|---|---|---|
| | $E_a$ (kcal/mole) | $D_o$ ($mm^2$/min) | $E_d$ (kcal/mole) | $D_o$ ($\times 10^4$ $mm^2$/min) |
| 130 | 7.32 | 18.0 | 10.68 | 1.1 |
| 150 | 8.78 | 166.1 | 11.39 | 3.5 |
| 180 | 9.79 | 985.8 | 10.59 | 1.0 |

chains, while the latter will depend on the segmental chain mobility. These two factors are also dependent on the degree of crosslinking of the polymer. It has been shown by Barrer and Skirrow[7] and later by Aitken and Barrer[8] that the energy of activation for diffusion and the pre-exponential factor also both increase with increasing crosslinking. These seem to lend support to the data shown in Table 8, in that different cure conditions do indeed result in different network structures for ATS.

## 3.1.6   Fracture Energies of ATS Polymer

Fracture energies of fully cured ATS polymers were measured. Specimens were cured initially to 90% conversion (as measured by DSC) at temperatures of 130, 150 and 180°C, respectively. They were then postcured at 300°C for 2 h, after which no futher polymerization reaction was detected by either DSC or TMA scans. This cure schedule served two purposes: (1) a complete fracture energy-temperature relationship can be ascertained without the interference of continuing cure in the sample during tests conducted at elevated temperatures and (2) the effect of various cure temperatures (130, 150 or 180°C) on network structures and thus the final state of cure, fracture energies of fully cured polymers can be investigated.

A method devised by Nakayama[9] and improved by Tattersall and Tappin[10] was used to measure the energy absorbed as a crack grows through a material.

The specimen is a square bar containing two cuts, put in by a diamond wafering blade, to reduce the square cross-section to an isosceles triangular cross-section. The load is applied through three rollers mounted on a platform. Figure 18 shows the shape of the specimen and the method of loading.
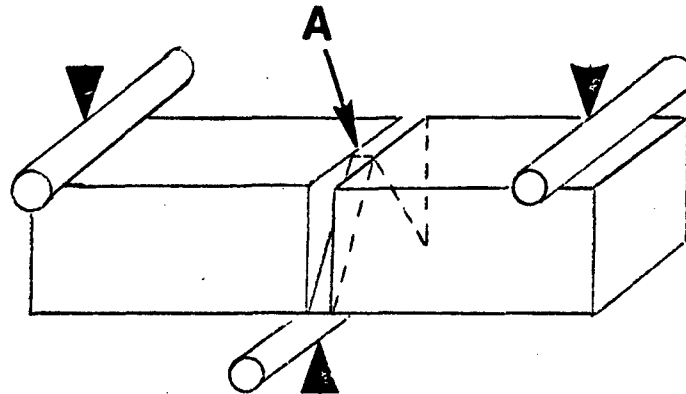


Fig. 18  Sample geometry for fracture energy measurements.

A sharp crack was initiated by tapping a new razor blade placed at the apex of the triangle. When a load is applied, a stress-concentration of sufficient magnitude develops at the top of the triangular cross-section (A), so that the precrack can be reinitiated before sufficient elastic energy is available to break the specimen completely. Further crack growth takes place in a controlled manner if the potential energy of the system is increased by deflecting the specimen by moving the crosshead. The work of fracture of the specimen, which is represented by the area under the load versus deflection curve, is the surface energy of the specimen, $\lambda_F$. The critical strain energy release rate of the specimen at fracture, $G_{1C}$, as shown by Sih and Liebowitz,[11] is given by Eq. (8):

$$2\lambda_F \; l = G_{1C} \quad . \tag{8}$$

The fracture energies of the fully cured samples as a function of test temperature are shown in Fig. 19. Also included for comparison are those of Narmco 5208. The data show that the fracture energies stay relatively unchanged until above 200°C, then they increase rapidly, maximizing around the glass transition temperature and drop precipitateously beyond the Tg. The data also show that ATS is consistently more brittle than Narmco 5208, a serious drawback if it is to be considered for structural applications.
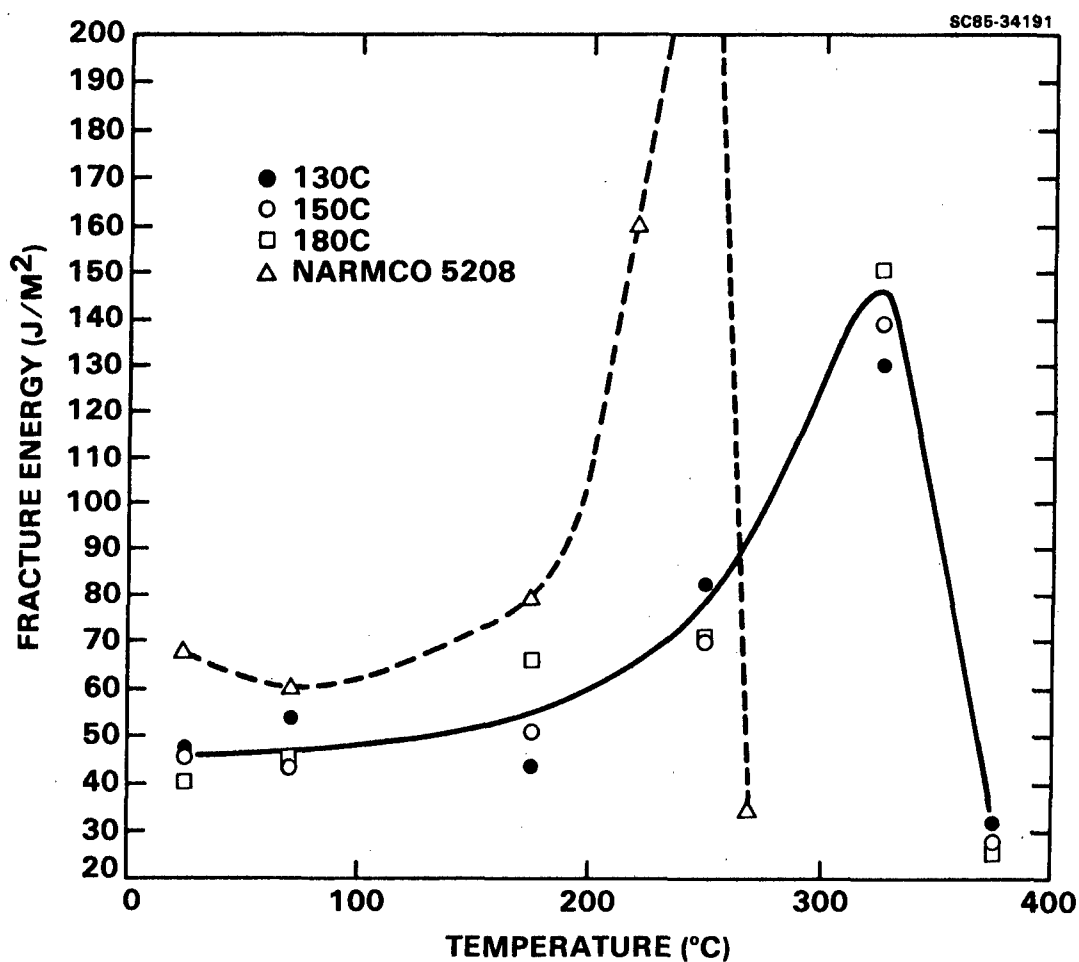


Fig. 19 Fracture energies of ATS as a function of temperature and cure conditions as determined by residual exotherm.

A more serious disappointment, however, is the fact that the data does not reveal a consistent cure path effect on fracture energies. One would expect specimens cured at low temperature prior to postcure to have a different network structure than specimens cured at a higher temperature. For the three cure temperatures presented in Fig. 19, a consistent trend is not observed.

A simple explanation can be made to clarify the apparent inconsistency if one assumes that maybe the specimens were at different cure states prior to the 300°C postcure step. Indeed, in a previous Section, data were presented showing discrepancies between thermal and spectroscopic determinations of degrees of cure. Due to the unequal states of cure prior to the 2 hours postcure at 300°C, a cure path effect on fracture energies therefore did not manifest itself in Fig. 19.

In order to ascertain the effect of cure paths and the resulting cure states on the structure-property relationship of ATS, the following new cure schedules were implemented.

| Cure Temperature (°C) | Time for Degree of Cure (via FTIR) (Min) | | |
|---|---|---|---|
| | 20% | 50% | 70% |
| 130 | 180 | 420 | 2700 |
| 150 | 75 | 170 | 320 |
| 180 | | 20 | 55 |

The above samples were cured according to the above schedule and then postcured at 250, 270 and 300°C, respectively, for 2 h to essentially 100% conversion. Thus, the new schedule encompasses a much more extensive range of cure conditions than were available previously. Additionally, the specimens cured at a particular temperature would all have equivalent degrees of cure prior to the postcure step.

Fracture energies were measured as previously described and are tabulated in Table 9.

Table 9

Fracture Energies of ATS Polymer at Various Cure States

| Cure Condition | Postcure Condition | $(J/m^2)$ |
|---|---|---|
| 130°C → 20% | 2 h @ 250°C | 34.6 |
| 130°C → 50% | 2 h @ 250°C | 34.0 |
| 130°C → 70% | 2 h @ 250°C | 39.0 |
| 150°C → 20% | 2 h @ 250°C | 35.0 |
| 150°C → 50% | 2 h @ 250°C | 36.1 |
| 150°C → 70% | 2 h @ 250°C | 33.8 |
| 180°C → 50% | 2 h @ 250°C | 35.9 |
| 180°C → 70% | 2 h @ 250°C | 36.0 |
| 130°C → 20% | 2 h @ 270°C | 37.1 |
| 130°C → 50% | 2 h @ 270°C | 38.0 |
| 130°C → 70% | 2 h @ 270°C | 40.9 |
| 150°C → 20% | 2 h @ 270°C | 37.0 |
| 150°C → 50% | 2 h @ 270°C | 33.2 |
| 150°C → 70% | 2 h @ 270°C | 36.2 |
| 180°C → 50% | 2 h @ 270°C | 34.2 |
| 180°C → 70% | 2 h @ 270°C | 34.0 |
| 130°C → 20% | 2 h @ 300°C | 25.8 |
| 130°C → 50% | 2 h @ 300°C | 37.2 |
| 130°C → 70% | 2 h @ 300°C | 45.5 |
| 150°C → 20% | 2 h @ 300°C | 32.1 |
| 150°C → 50% | 2 h @ 300°C | 30.2 |
| 150°C → 70% | 2 h @ 300°C | 40.8 |
| 180°C → 50% | 2 h @ 300°C | 31.5 |
| 180°C → 70% | 2 h @ 300°C | 32.1 |

Figure 20 shows that although there is a considerable amount of scatter in fracture energies among the three cure temperatures, a distinct improvement is obtained when the resin was cured to a high percent of conversion at comparatively low temperatures, i.e., 130 or 150°C, than when cured at 180°C. The fracture energies of the best samples, however, are still below those of the baseline epoxy (Narmco 5208). This contrasts with the results obtained at AFWAL[18] where the $K_Q$ (as measured by the compact tension geometry) of ATS does not seem to vary as a function of cure conditions.
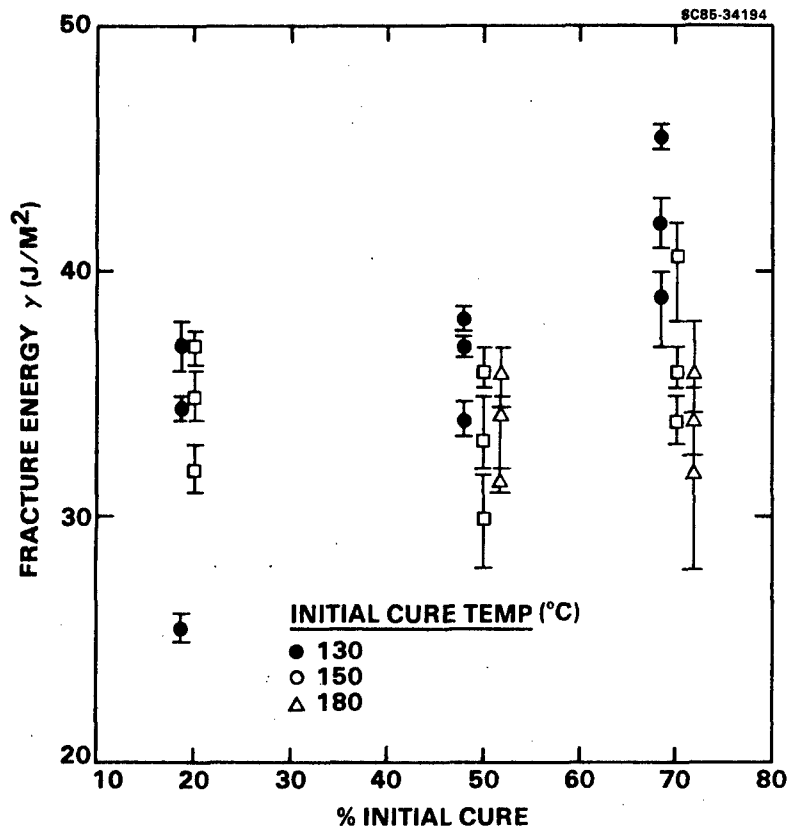
Fig. 20  Fracture energies of ATS as a function of temperature and
cure conditions as determined by FTIR.

### 3.1.7  Tensile Properties of ATS

Stress-strain properties of ATS polymers at different cure states were measured. Specimens were cured in silicone molds in the form of standard microtensile specimens and cured to 90% (as measured by DSC residual exotherms) at 130, 150 and 180°C, respectively, then postcured to 100% at 300°C for 2 h. Tests were performed in an environmental chamber at ambient relative humidity and at temperatures of 23, 100, 200, 300 and 370°C, respectively. The data therefore covered the entire glassy to rubbery regions, as the glass transition temperatures of the fully cured ATS polymers has been previously determined to be at 350°C.

31

Table 10 tabulates the tensile properties of the ATS polymers. The data are plotted in the form of failure envelopes for each cure temperature as shown in Fig. 21.

Table 10

Tensile Properties of ATS Polymers

| Cure Temperature (°C) | Test Temperature (°C) | $\sigma_b$ | | $\varepsilon_b$ |
|---|---|---|---|---|
| | | (kg/cm$^2$) | (MPa) | (%) |
| 130 | 23 | 403 | 39.5 | 2.1 |
| | 100 | 378 | 37.1 | 2.6 |
| | 200 | 377 | 36.9 | 4.1 |
| | 300 | 310 | 30.4 | 4.6 |
| | 370 | 185 | 18.1 | 4.9 |
| 150 | 23 | 405 | 39.7 | 2.5 |
| | 100 | 382 | 37.5 | 2.6 |
| | 200 | 360 | 35.3 | 2.8 |
| | 300 | 310 | 30.4 | 3.4 |
| | 370 | 170 | 16.6 | 4.3 |
| 180 | 23 | 409 | 40.1 | 2.0 |
| | 100 | 372 | 36.5 | 2.1 |
| | 200 | 321 | 31.5 | 2.5 |
| | 300 | 298 | 29.2 | 3.6 |
| | 370 | 200 | 19.6 | 4.4 |

The shapes of the failure envelopes are in agreement with those obtained by Eddy, et al.[12] One important feature is the difference in failure response exhibited by the three cure temperatures. This signifies the difference in network structure resulted from the different cure conditions.

3.1.8 Accelerated Aging of ATS

Specimens cured to 90% (as measured by DSC residual exotherms) at 130, 150 and 180°C and postcured at 300 C for 2 h were aged in an air circulating oven set at 250°C. Samples were removed at certain time intervals and the room

SC82-17123
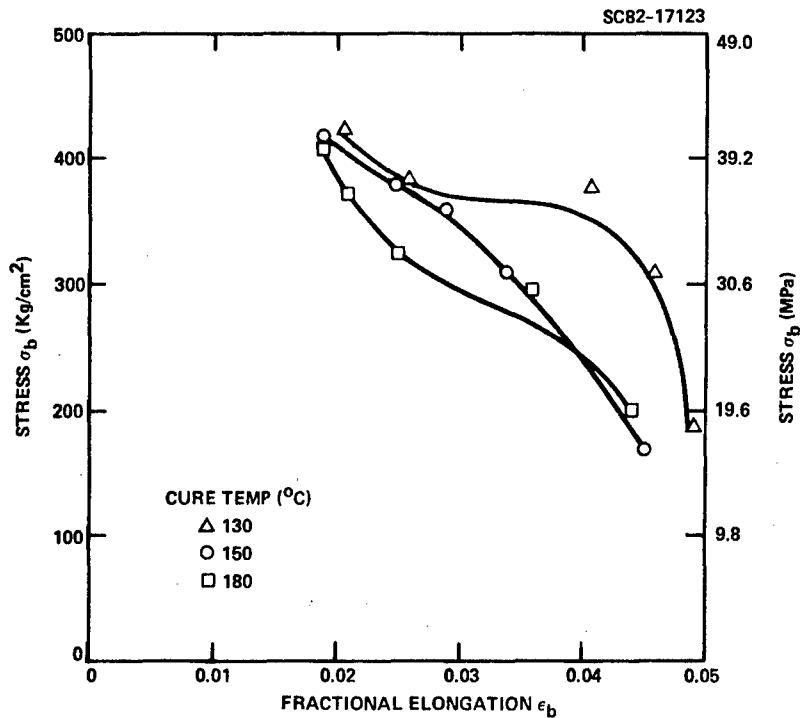


Fig. 21   Failure envelope of fully cured ATS.

temperature fracture energies of these samples were then measured.  The results
are summarized in Table 11.

The data show that up to about 1000 hours, ATS appears to be quite
stable and lost only about 10% of its fracture energies.  After about 2600
hours, however, close examination of the specimens showed many surface cracks
which, although did not penetrate too deeply into the interior, might have
caused the lowering (20-30%) of the fracture properties of the specimens.

### 3.1.9   Computer-Aided Analysis of ATS Polymers

Computer-based models were applied to develop relations between the
chemical structure of acetylene terminated polysulfone resin and the thermome-
chanical response as a function of cure states.  The glass transition tempera-
ture of the ATS increases with cure along a theoretical curve characteristic of
chain extension and branching from zero to 80% of complete cure.  Between 80%
and complete cure the Tg rises abruptly from 150°C to a final value of 350°C for

33

Table 11

Fracture Energies of ATS After Aging at 250°C in Air

| Cure Temperature (°C) | Aging Time (h) | $\gamma_F$ (J/m$^2$) |
|---|---|---|
| 130 | 0 | 47 |
|  | 120 | 46 |
|  | 936 | 44 |
|  | 2592 | 38 |
| 150 | 0 | 49 |
|  | 120 | 50 |
|  | 936 | 46 |
|  | 2592 | 39 |
| 180 | 0 | 55 |
|  | 120 | 52 |
|  | 936 | 50 |
|  | 2592 | 38 |

the fully cured resin, as shown in Fig. 22. The chemical structure of cured ATS resin was introduced into a computer-based model for numeric estimation of time dependent modulus, tensile strength, extensibility and unnotched fracture energy. The computed fracture energy (unnotched) and measured fracture energy (notched) are shown to display similar thermal response from 23 to 375°C, as shown in Fig. 23.

Chemical modelling of ATS tensile properties has also been carried out. Two notable features of the theoretical modelling and experimental results are: (1) The maximum tensile strength for brittle fracture at low temperature is lower than that predicted by the structure-property predictive model. The experimental results are lower by a factor of two to three. (2) The maximum tensile extensibility at high temperature (near the Tg) is well below the predicted value by a factor of two to three. The chemical structure model for ATS associates the brittle failure strength with the polymer cohesive energy density whose calculated value is $\delta^2$ = 121.6 cal/cc. On the assumption that the sulfone groups form an intermolecular complex and do not contribute to interchain cohesion, the "effective" ATS cohesive energy is then lowered to $\delta^2$ = 62.4 cal/cc.
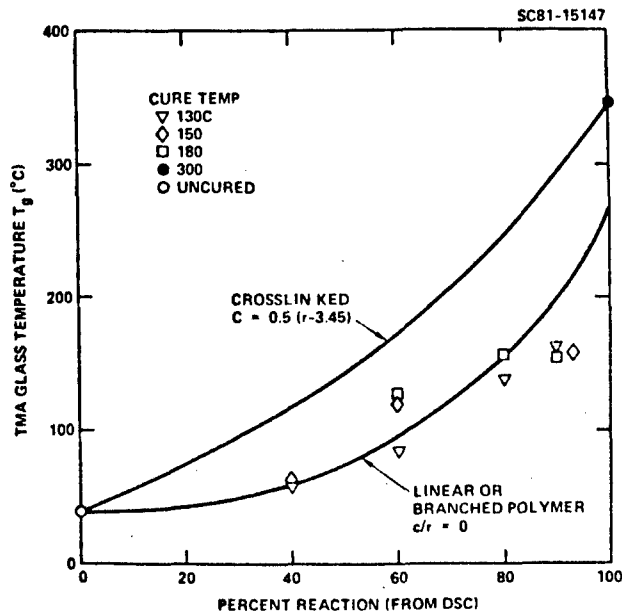
Fig. 22 Analytical modelling of glass transition
temperature of ATS during cure.
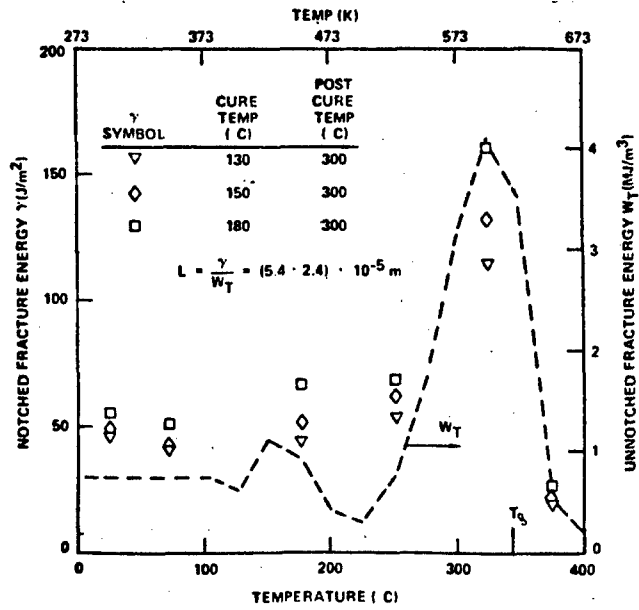
Fig. 23 Analytical modelling of fracture energies of
ATS during cure.

On the further assumption that the hypothetical sulfone intermolecular complex behaves as a physical crosslink, the "effective" molecular weight between crosslinks, $M_c$, is reduced from a calculated value of $M_c$ = 1817 g/mole to a new value of $M_c$ = 450 to 900 g/mole. The latter value is related to the molecular spacing and coordination between the sulfone groups.

The new values of $\delta^2$ = 62.4 cal/cc and $M_c$ = 904, 678 and 565 g/mole, respectively, were then introduced into computer simulations of tensile stress-strain response, as shown in Figs. 24 to 26. The figures show that the maximum tensile extensibilities diminish from 0.16 to 0.044 as $M_c$ is reduced from 904 g/mole to 505 g/mole. The maximum experimental extensibilities of 0.04 at temperatures above the Tg is therefore in agreement with Fig. 26 which depicts an effective $M_c$ = 560 g/mole. The tensile strengths of 180 to 400 kg/cm$^2$ measured at 200 to 370°C are also in agreement with the calculated values as shown in the figures.

SC83-25348

STRESS vs STRAIN - TENSILE, ENHANCED - FIXED T = 1.00 SEC
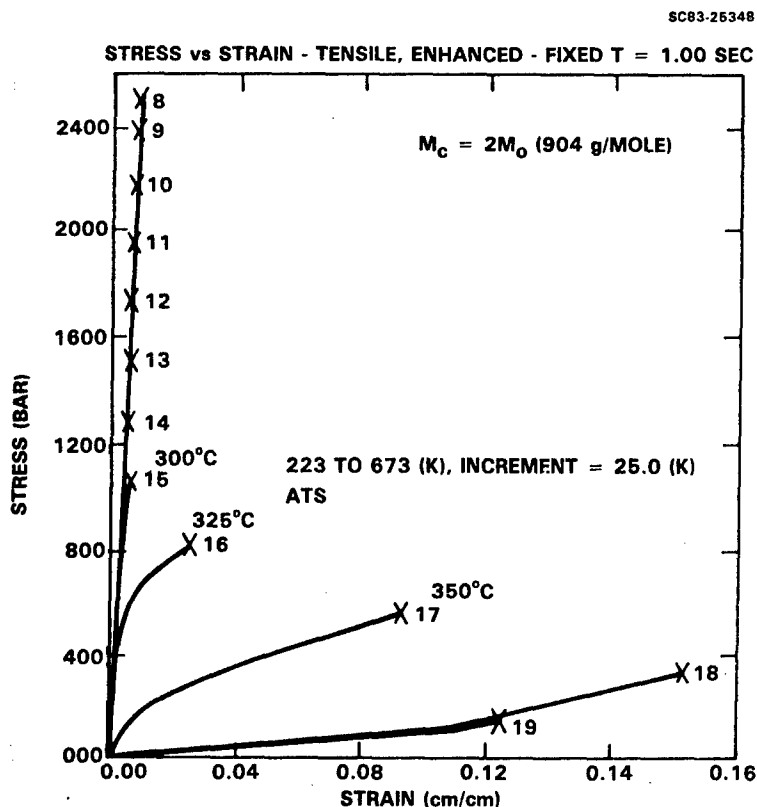


Fig. 24 Analytical modelling of tensile properties of ATS ($M_c$ = 904 g/mole).

**STRESS vs STRAIN - TENSILE, ENHANCED - FIXED T = 1.00 SEC**

$M_c = 1.5M_0$ (678 g/MOLE)

300°C

325°C    223 TO 673 (K), INCREMENT = 25.0 (K)
         ATS

350°C

STRESS (BAR)

STRAIN (cm/cm)
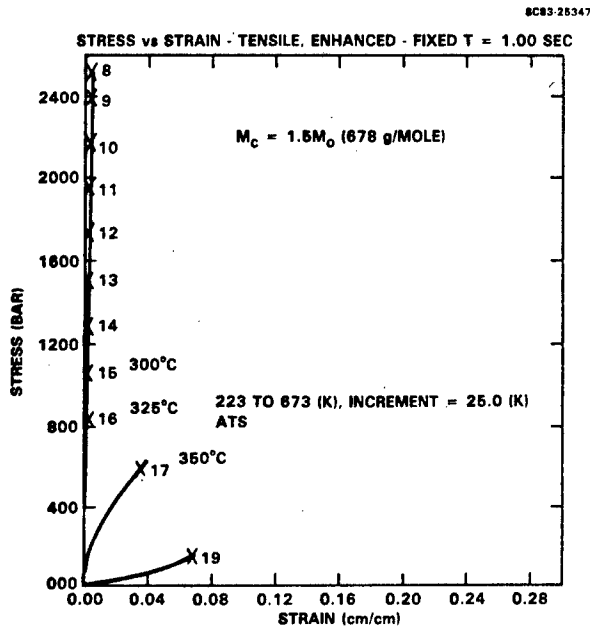
Fig. 25   Analytical modelling of tensile properties of ATS
          ($M_c$ = 678 g/mole).

175°C AND BELOW

200°C

225°C

250°C

275°C

300°C

325°C

STRESS (BAR)

STRAIN (cm/cm)

223 TO 673 (K), INCREMENT = 25.0 (K)
ATS-SULFONE-COMPLEXED-ITG = 344C)
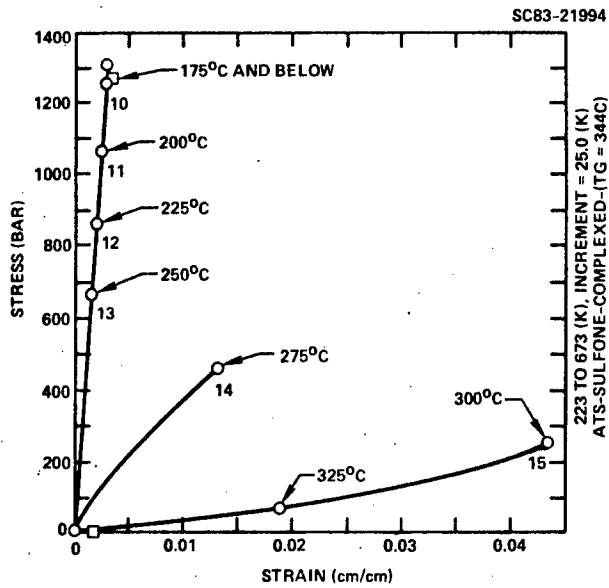
Fig. 26   Analytical modelling of tensile properties of ATS
          ($M_c$ = 565 g/mole).

37

The theoretical value of $M_c$ = 565 g/mole is very close to the monomeric molecular weight of ATS (480 g/mole), lending support to the "cluster model" proposed for the structure of cured ATS.[13] In this proposed model, two molecules of ATS initiate the propagation of one acetylene per monomer unit into a polyene. This results in a cluster-shaped species the growth of which is inhibited by the steric hindrance of the pendant groups. Subsequent polyene formation thus results in a crosslinked structure with $M_c \simeq M_o$.

Many other mechanisms for the brittle response of ATS can be proposed. However, the notion of a sulfone group complex provides a simple mechanism which when introduced into a polymer predictive model appears to correlate with experimental results in the tensile failure envelopes of cured ATS.

## 3.1.10    Composite Fabrication

### 3.1.10.1 Unidirectional Laminates

Prepregs of ATS/Celion 12K were prepared by a modified pultrusion method with the resin maintained at about 80°C throughout the operation. A description of the prepregging operation is detailed in the Appendix. A 15 ply laminate was laid up, degassed and compacted in vacuum at 90-100°C for about 1 h, as shown in the upper portion of Fig. 27. The resin content of the prepreg was calculated to be 38% by weight.

Laminates were cured using the "no bag" technique shown in the lower portion of Fig. 27. A laminate was simply placed on a caul plate with a single ply of porous Teflon release ply on each side and cured under a constant air pressure of 120 psi. The cure cycle was previously developed at the Materials Laboratory:[14] 24 h at 140°C, 1 h at 200°C, followed by a postcure of 10 h at 300°C. Neat resin specimens prepared by this cure cycle was shown to have improved room temperature tensile properties: tensile strength of 9.8 ksi and tensile elongation of 2.06%.

Cured composites were ultrasonically C-scanned, as shown in Fig. 28, in which no interior void or delamination was observed. Polished micrographs, as shown in Fig. 29, revealed that the fibers were fairly well distributed
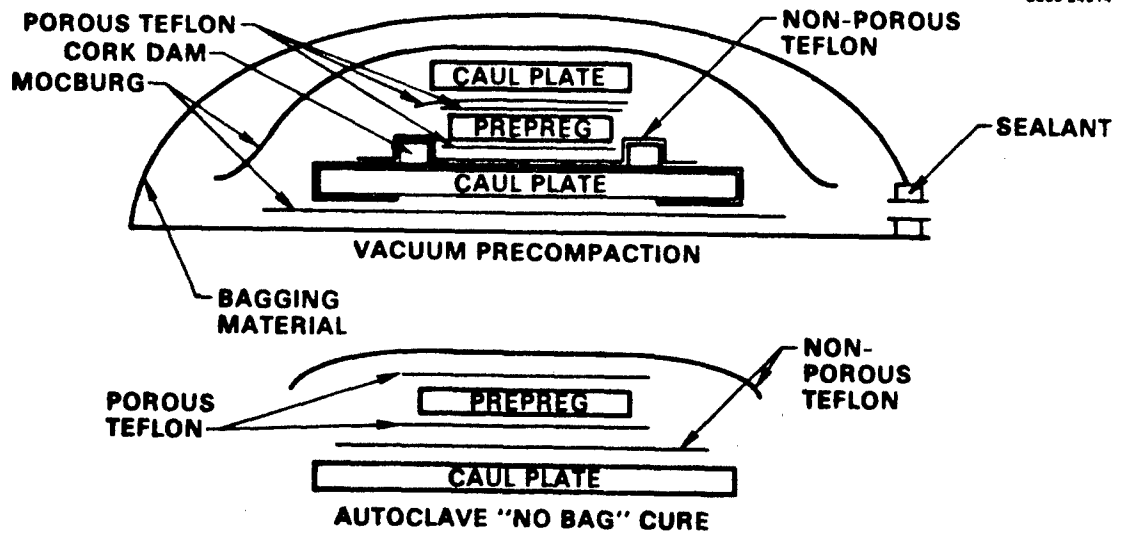
Fig. 27 Schematic of vacuum precompaction and "no bag" autoclave cure.
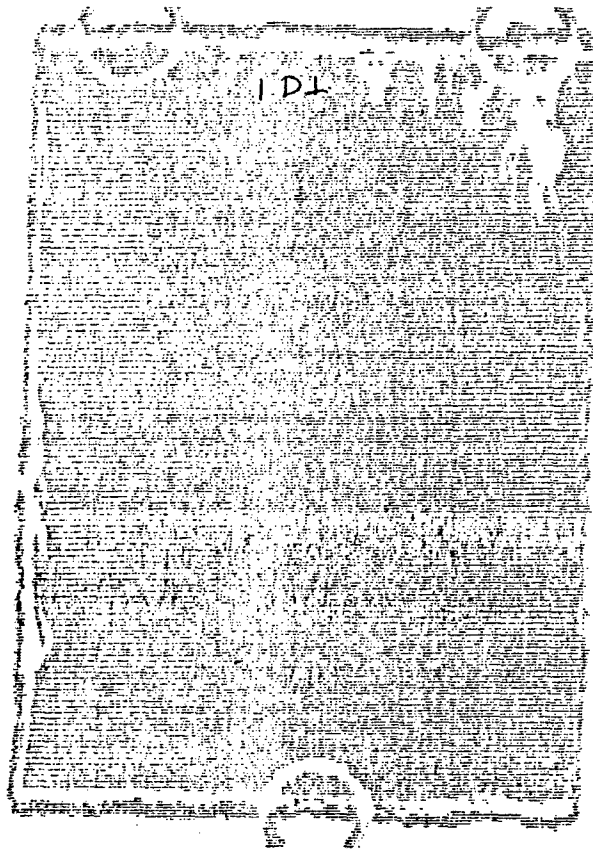


Fig. 28 C-scan of unidirectional ATS/Celian 12K laminate.
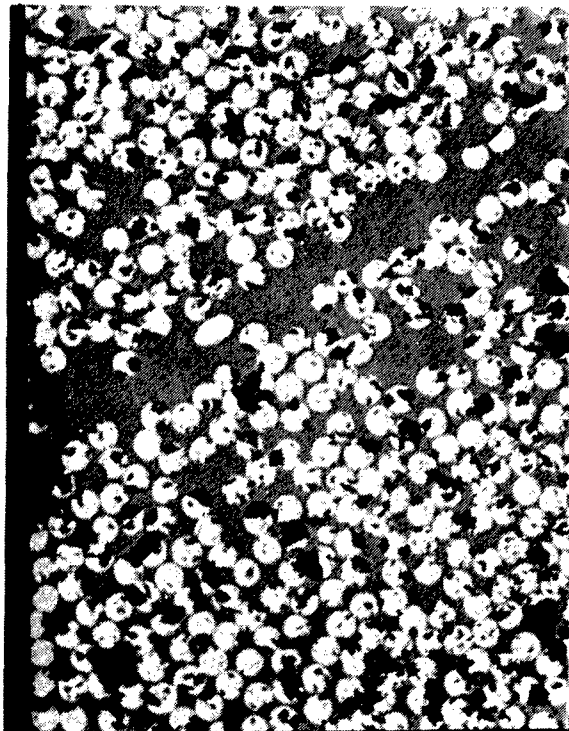
Fig. 29   Polished edge micrograph of ATS/Celian 12K laminate.

Comparable values were obtained for AS4/m-ATS:[3]

Four-point interlaminar shear strength: 62 MPa (9.1 ksi).

Three-point flex strength: 1.4 GPa (198 ksi); modulus 132 GPa
(19.2 msi).

Four-point 90° flex: 49.6 MPa (7.2 ksi); modulus 9.0 GPa (1.3 msi).

Scanning electron microscopy studies were performed on the fracture
surfaces of the composites.  Figure 30 shows the scanning micrographs of the
composite failure surface from the four-point interlaminar shear test.  Perhaps
because the Celion fibers are unsized, the adhesion of the matrix to the fiber
·is only fair, as evidenced by the bare fiber surfaces, some with striations
clearly visible (area A in Fig 30a).  In areas where the fiber has detached from
the matrix, concave impressions with the striations are clearly visible (area A
in Figs. 30b and 30c).  Throughout the fracture surface, hackles traversing the

40

Three-point flex strength: 1.4 GPa (198 ksi); modulus 132 GPa (19.2 msi).

Four-point 90° flex: 49.6 MPa (7.2 ksi); modulus 9.0 GPa (1.3 msi).

Scanning electron microscopy studies were performed on the fracture surfaces of the composites. Figure 30 shows the scanning micrographs of the composite failure surface from the four-point interlaminar shear test. Perhaps because the Celion fibers are unsized, the adhesion of the matrix to the fiber is only fair, as evidenced by the bare fiber surfaces, some with striations clearly visible (area A in Fig 30a). In areas where the fiber has detached from the matrix, concave impressions with the striations are clearly visible (area A in Figs. 30b and 30c). Throughout the fracture surface, hackles traversing the matrix between two adjacent fibers are seen (area C in Fig. 30b and 30c, for example), although the amount of hackles are considerable less than those observed on state-of-the-art epoxies. This is indicative of the brittle nature of fully cured ATS.

Fracture surfaces of the transverse flexure test are shown in Fig. 31. The micrographs show that fracture occurred mainly within the matrix, leaving the fibers still encased by the resin. Hackles in the matrix resin are still visible, as shown by area A in Fig. 31b. Figure 31c shows a magnified view of the hackles.

### 3.1.10.2 Cross-Ply Laminates

Laminates consisting of 14 plies, each ply being 90° to the previous, were fabricated. The purpose of this configuration is to maximize the internal stress due to the orthogonality of ply orientation and to look for microcracking in the cured composite. After the panels were cured at 140°C for 24 h, followed by 177°C for 5 h, a portion of the panel was sectioned and edge-polished. Optical micrographs, shown in Fig. 32, failed to reveal any observable cracks through the panel thickness. Therefore, it is concluded that even though a faint crackling sound was heard during the cool-down from 177°C to room temperature, the microcracks generated, if any, were well below observable sizes.
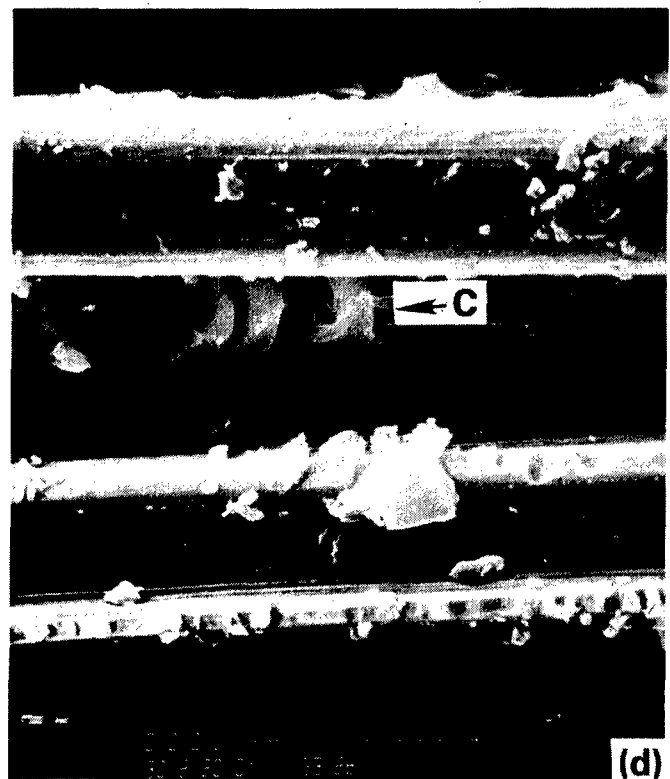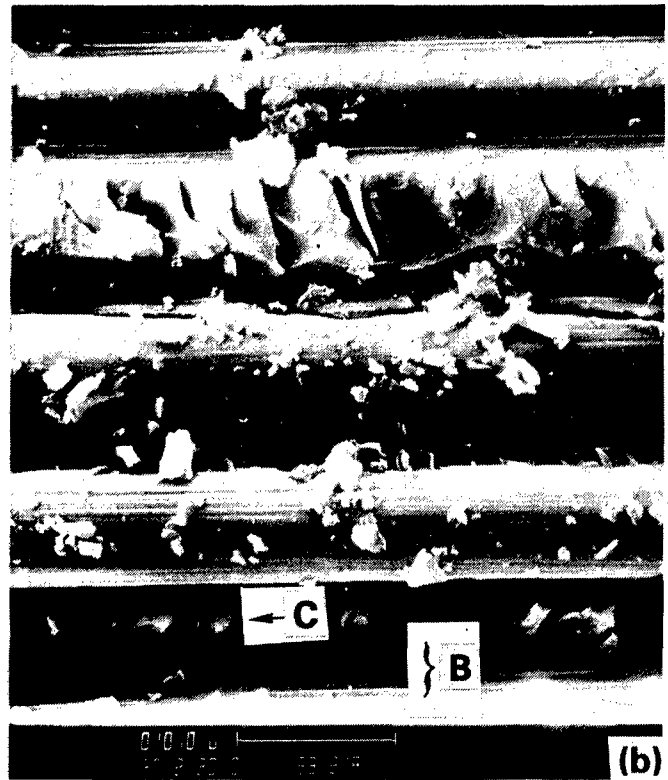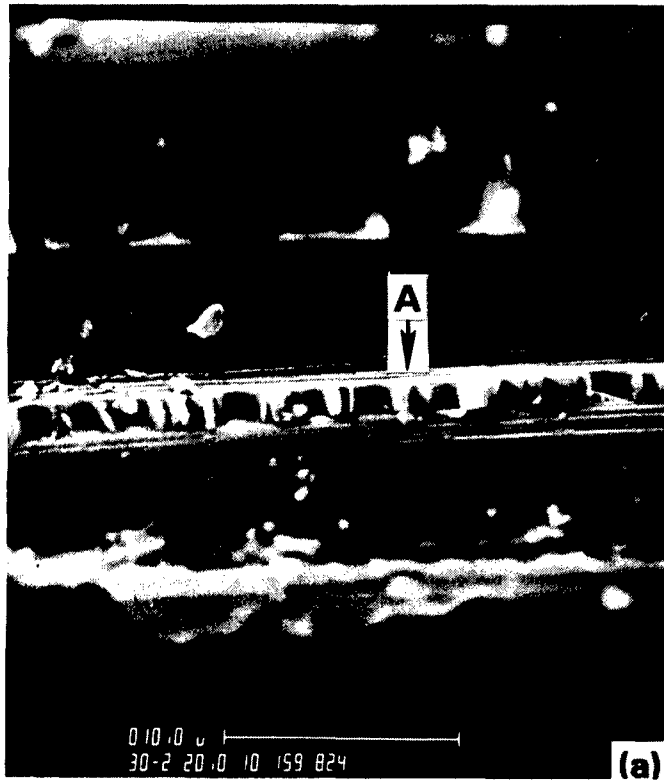
Fig. 30 Scanning electron micrographs of four-point interlaminar
shear fracture surface of ATS/Celian 12K laminate.
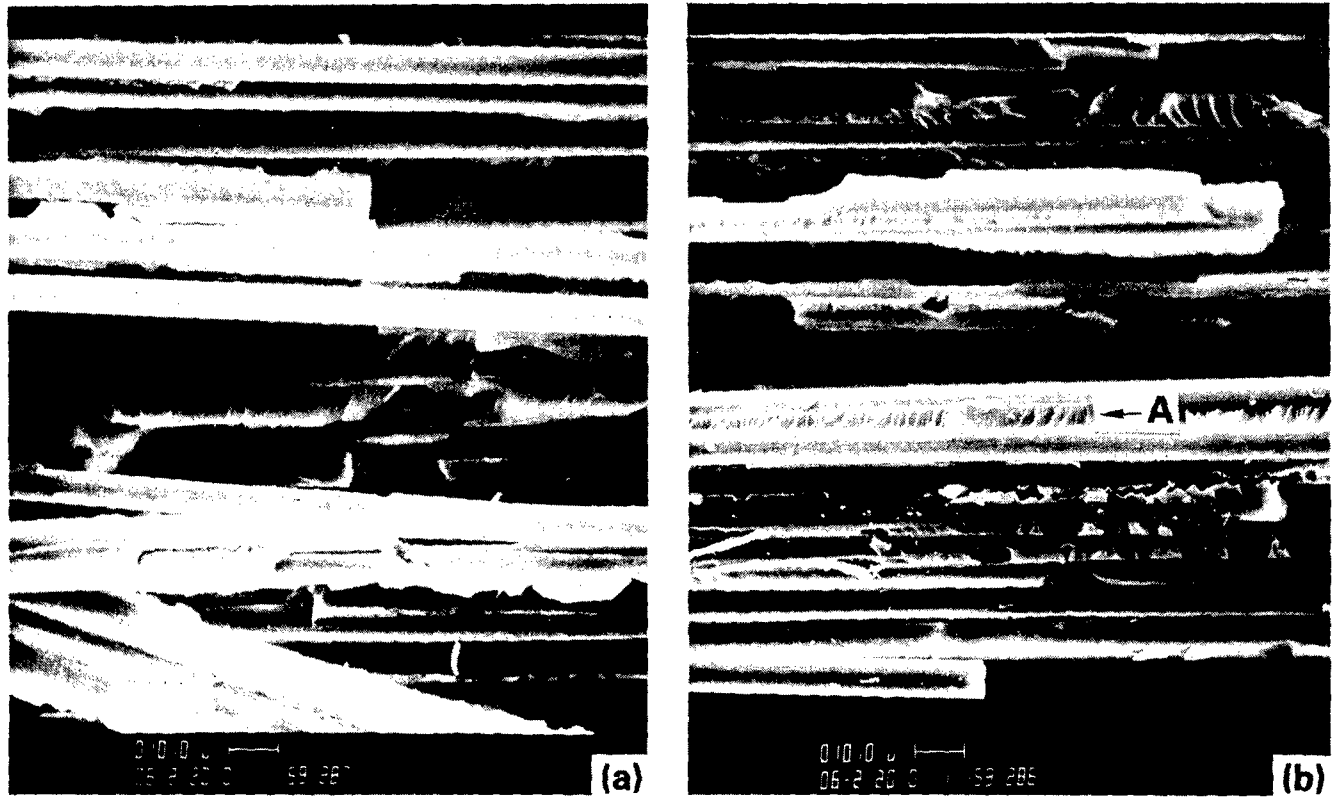
Fig. 31   Scanning electron micrographs of transverse flex failure
surface of ATS/Celian 12K laminate.
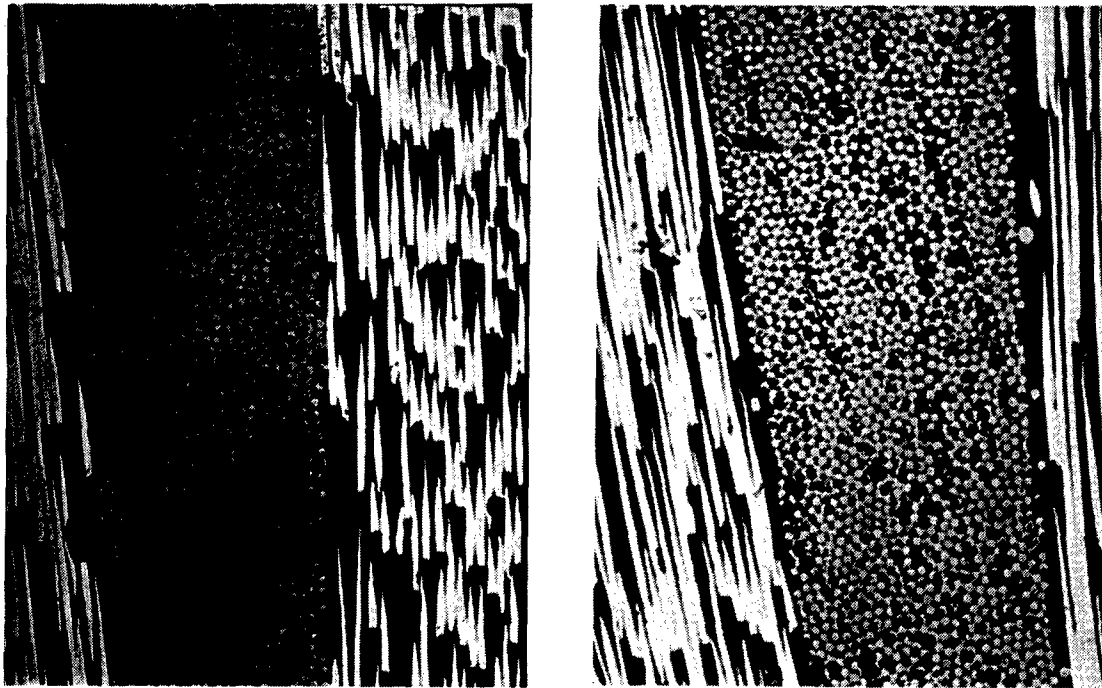
**250X**
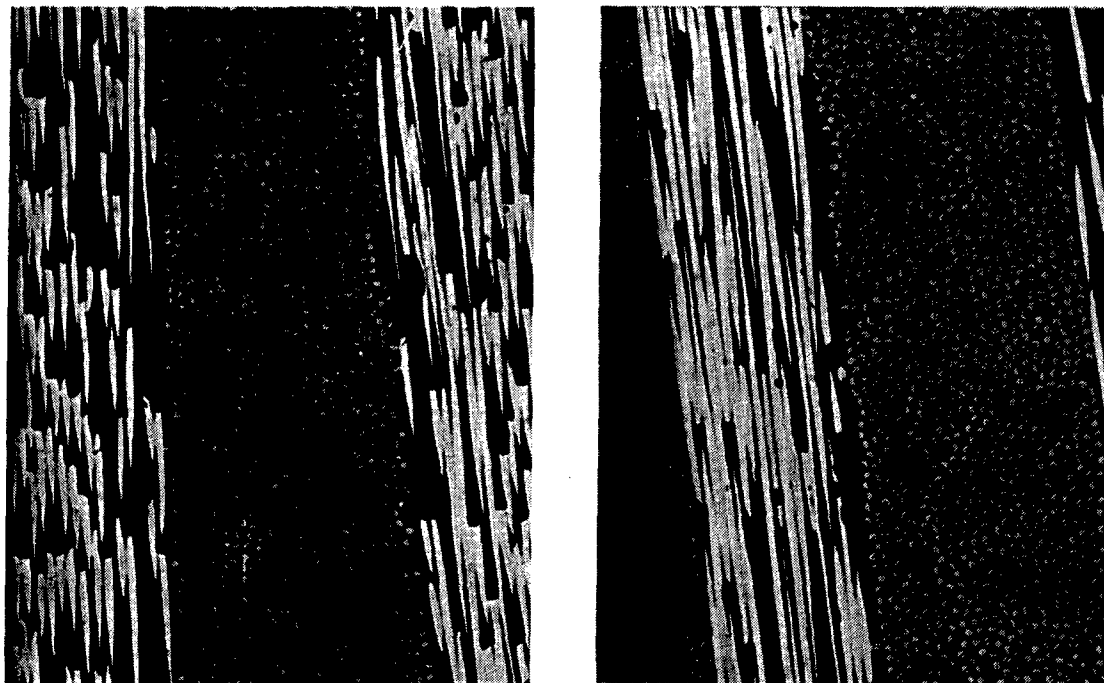
Fig. 32   Polished edge micrograph of [0,90 ]$_{14}$ ATS/Celian 12K laminates, cured at 140°C for 24 h and 117°C for 5 h.

The remaining portions of the panel were then post-cured at 300°C for 10 h. Fiber volume of the panels were found to be 55%. Samples measuring 0.5 inch by 4 in. were cut from the panels so that the fibers are aligned in a +45 orientation with respect to the long dimension. Tensile strength of the +45 specimens were measured at room temperature at a crosshead speed of 0.1 mm/min. Strain was measured by extensiometer. Using the following relation,

$$S = P/2bd$$

where

S = ultimate unidirectional in-plane shear strength

P = maximum load (force) on the load-deflection curve

b = width of specimen

d = thickness of specimen,

the average in-plane shear strength of the +45 ATS composite was calculated to be 51.7 MPa (7.5 ksi), with an average tensile strain of 5%. A typical value for structural epoxy is about 67.9 MPa (9.5 ksi), again indicating the relatively brittle nature of the ATS resin.

## 3.2    Tertiary Blends of ATS/ATP/HR600P

The thermophysical and low moisture uptake of acetylene terminated polysulfones (ATS), especially at elevated temperatures, have been shown to be superior to other thermosets, e.g., epoxies. However, low fracture toughness and poor tack and drape remain as some of the problem areas for ATS.

Difunctional acetylene terminated phenylene oxide (di-ATP) has been found to be extremely useful in providing the necessary chain flexibility to increase the fracture toughness of ATS when ATP is used as a diluent.[15]

The fracture toughness of HR600P has been shown to be better than that of ATS.[16] Accordingly, the feasibility of improving the fracture toughness and processibility of ATS by the blending of itself into ATP and HR600P is studied. The plan calls for the following:

(1) Determine the compatibility of ATS-ATP, ATS-HR600P and ATS-ATP-HR600P mixtures.

(2) Blend various ratios of ATP-HR600P, acting as diluents, into ATS, at a ratio of ATS diluent = 70/30 and 50/50, respectively.

(3) Determine the rheological and thermophysical properties of the blended mixtures.

(4) Determine the appropriate cure cycles.

(5) Measure tensile properties of the cured polymer.

## 3.2.1 Thermophysical Properties of Tertiary Blends

Glass transition temperatures of the tertiary blends of ATS/ATP/HR600P were measured. The data were then compared with those calculated by the rule of mixtures:[17]

$$Tg \text{ (mixture)} = W_1(Tg)_1 + W_2 (Tg)_2 + KW_1W_2$$

where Wi is the weight fraction of each component, $Tg_{(i)}$ its glass transition, and K is a correction factor, usually taken to be 2. Table 12 tabulates the measured and calculated Tgs of the tertiary blends, using the values of Tg (ATS monomer) = 38°C, Tg (ATP monomer) = -43°C and Tg (HR600P monomer) = 130°C.

Table 12

Calculated and Experimental Glass Transition Temperatures
of Tertiary Blends of ATS/ATP/HR600P

| ATS/ATP/HR600P | Glass Transition Temperature (°C) | |
| --- | --- | --- |
| | Calculated | Measured |
| 70/9/21 | 50 | 43 |
| 70/21/9 | 29 | 20 |
| 50/25/25 | 41 | 32 |

Within experimental errors, it can be concluded that there is no significant phase separation between the components, and that the three components are compatible with each other in the blend.

Activation energies for the cure of the tertiary blends were measured by differential scanning calorimetry. Table 13 tabulates the activation energies of the blends.

Table 13

Activation Energies for the Cure of ATS/ATP/HR600P Blends

| ATS/ATP/HR600P | Ea (Kcal/mole) |
|---|---|
| 70/9/21 | 27.8 |
| 70/21/9 | 28.2 |
| 50/25/25 | 27.5 |

## 3.2.2 Rheological Characterization of Tertiary Blends

Dynamic viscosities of ATS blended with various ratios of ATP and HR600P were measured. The materials were dissolved in THF in the ratios of ATS/ATP/HR600P = 70/30/0, 70/0/30, 70/21/9, 70/9/21 and 50/25/25, respectively. The solutions were evaporated to dryness in a vacuum oven at about 90°C. Parallel plate viscometry was performed at 10 rad/s and at a scan rate of 2°C/min. Figures 33-38 show the dynamic viscosities, as well as the storage and shear moduli, of the blended resins. As expected, the addition of ATP into ATS lowered the viscosities of the blends, while the addition of HR600P increased the viscosities.

## 3.2.3 Dynamic Mechanical Properties of Tertiary Blends

Dynamic mechanical properties of two ATS tertiary blends with ratios of ATS/ATP/HR600P = 70/21/9 and 70/9/21, respectively, were measured. The rectangular specimens were cured in an autoclave, under 110 psi in nitrogen. This is necessary to prevent the volatilization of ATP during cure. Specimens were cured at 150°C for 24 h followed by 180°C for 6 h.
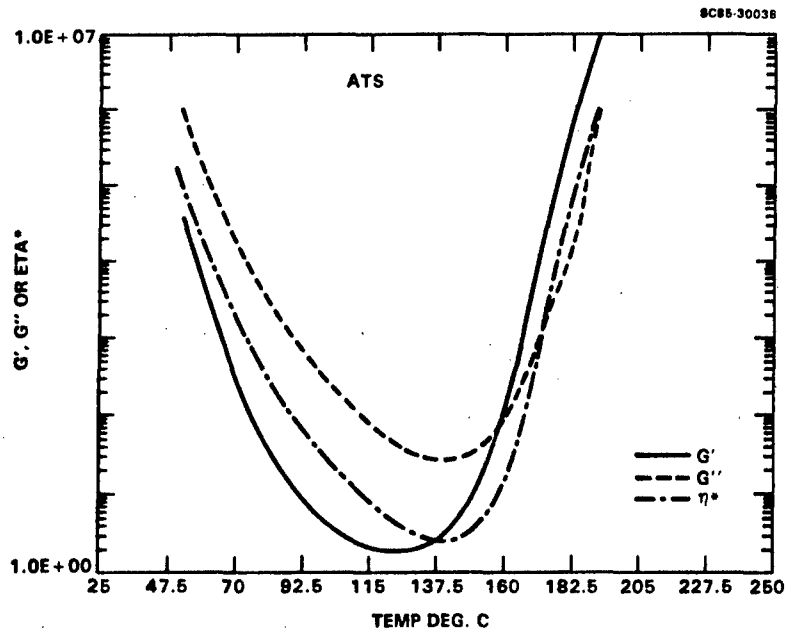
Fig. 33   Parallel plate rheometry of ATS.
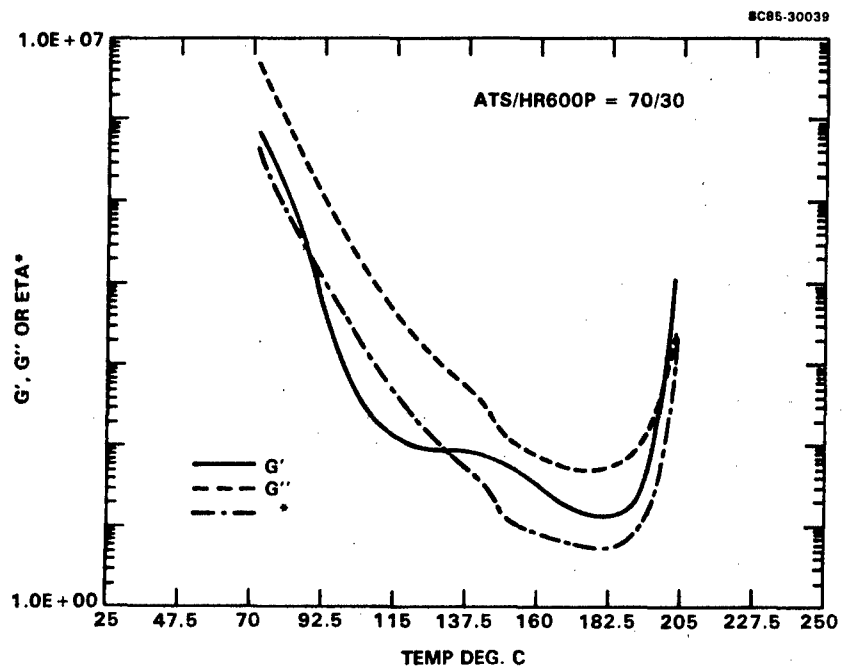


Fig. 34   Parallel plate rheometry of ATS/HR600P = 70/30.
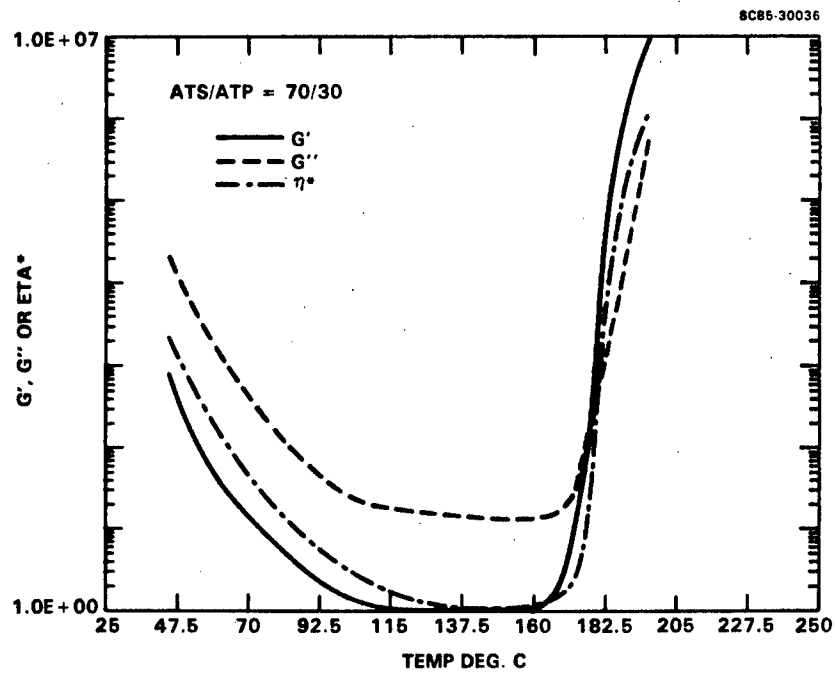
Fig. 35  Parallel plate rheometry of ATS/ATP = 70/30.
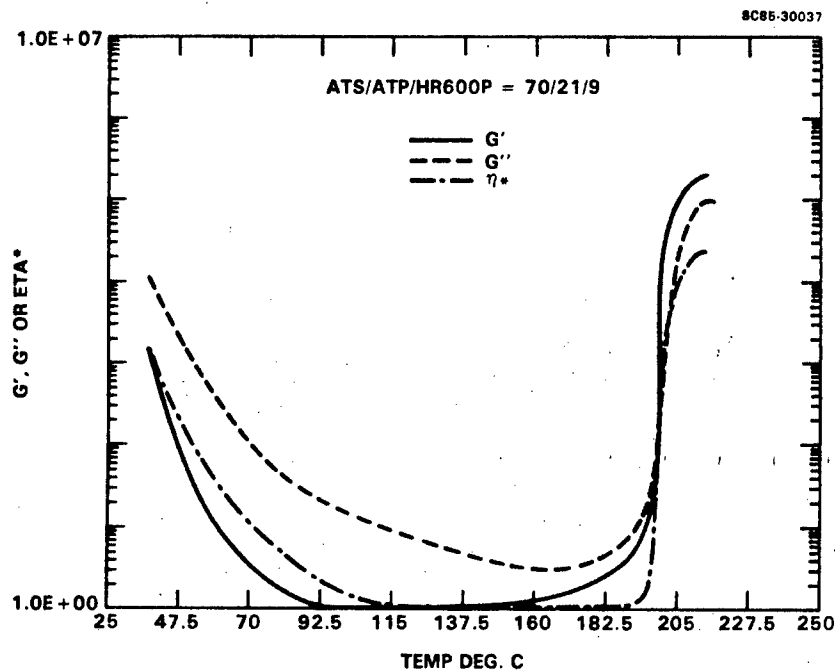
Fig. 36  Parallel plate rheometry of ATS/ATP/HR600P = 70/21/9.
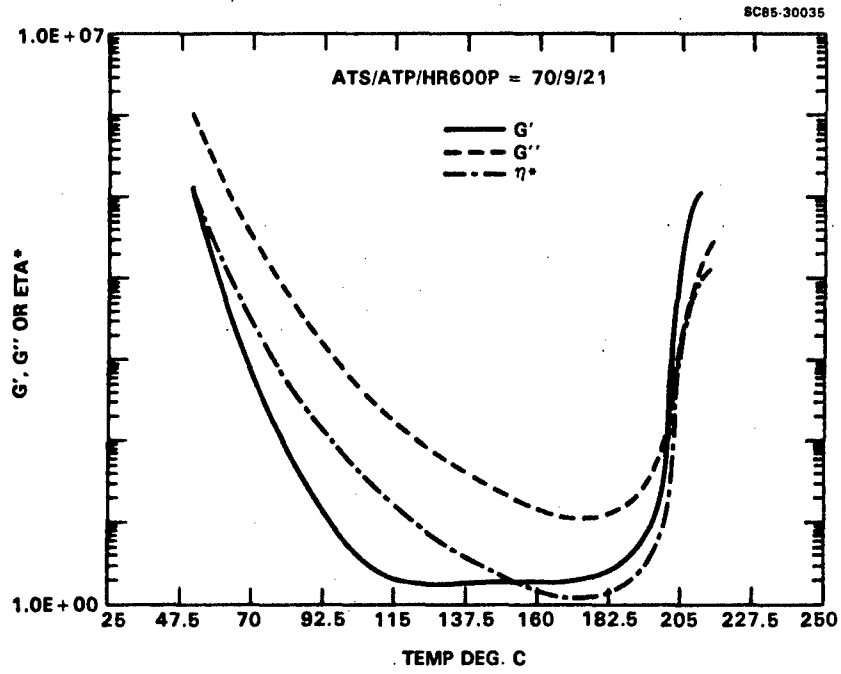
Fig. 37 Parallel plate rheometry of ATS/ATP/HR600P = 70/9/21.
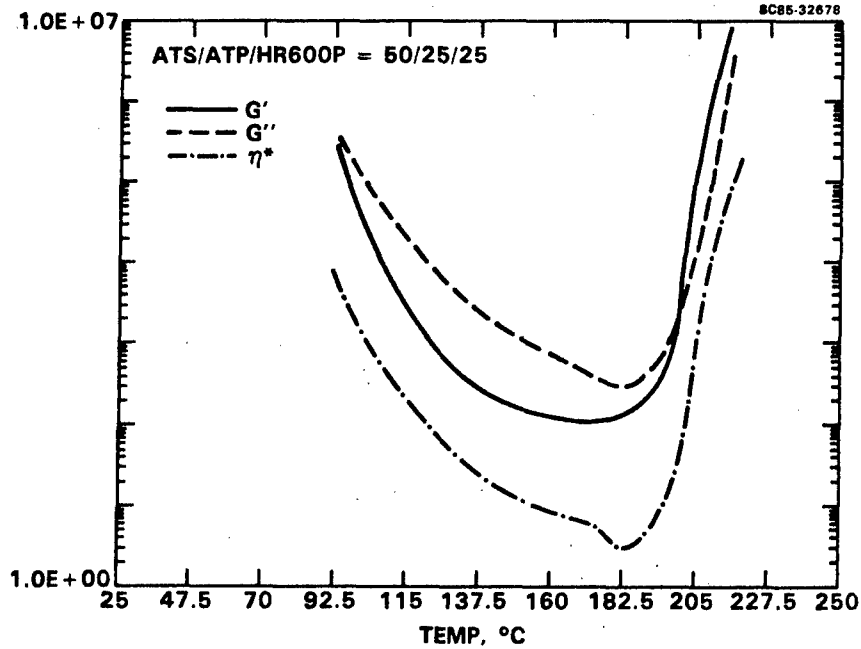


Fig. 38 Parallel plate rheometry of ATS/ATP/HR600P = 50/25/25.

Figures 39 to 42 show the dynamic mechanical spectra of the two blends when measured at 2°C/min and 10 rad/s in the torsional mode in the Rheometrics Mechanical Spectrometer. Essentially, there is a low temperature transition at about -100°C due to moisture in the ATS, a broad transition slightly above room temperature, followed by a glass transition at about 350°C. As expected, the blended materials show a lower Tg than that of ATS itself. The figures also show that increasing ATP concentration decreases slightly the Tg of the cured blend. Most importantly, however, is the absence of multiple transitions, indicating the compatibility of the various components of the blend.
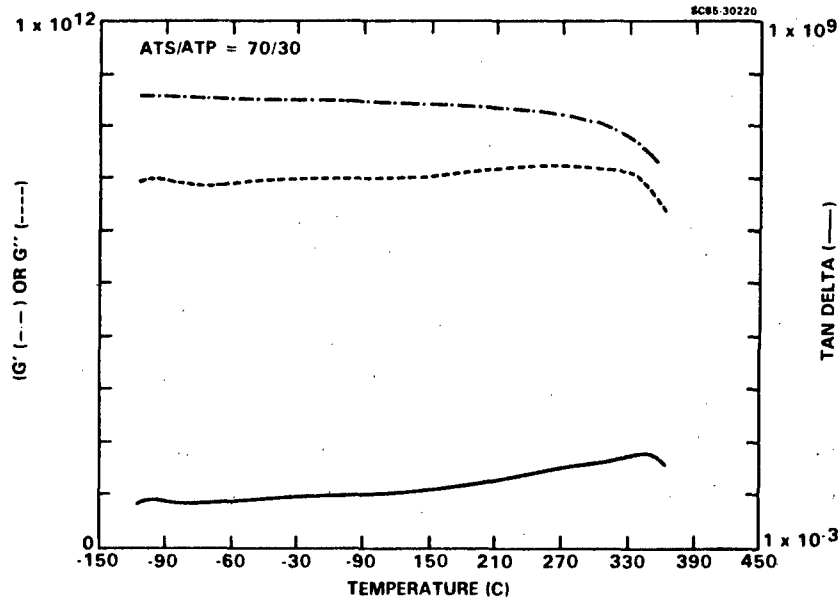


Fig. 39   Dynamic mechanical properties of ATS/ATP = 70/30.
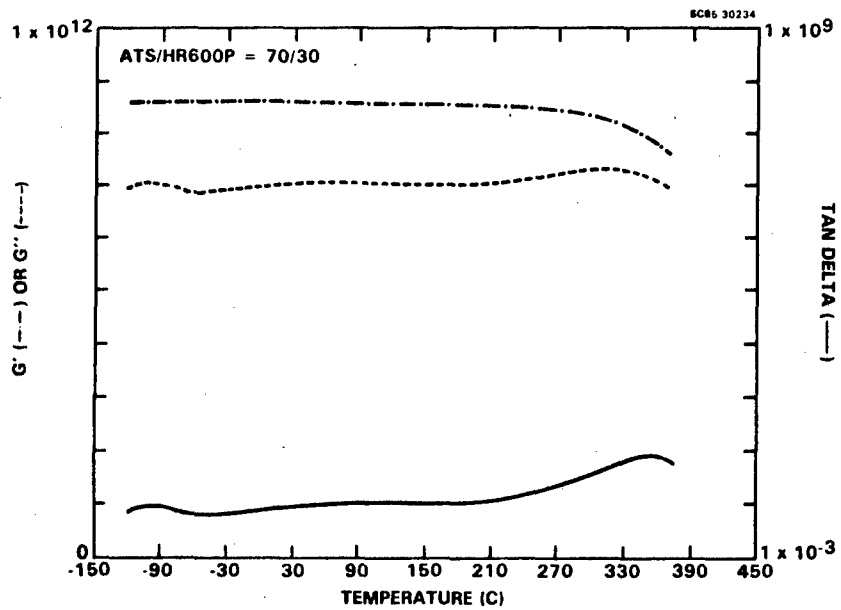
Fig. 40  Dynamic mechanical properties of ATS/HR600P = 70/30.
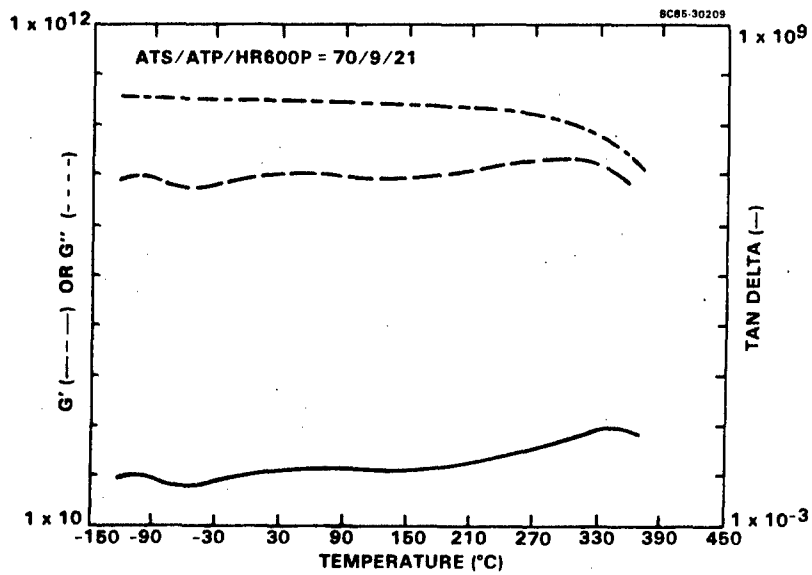


Fig. 41  Dynamic mechanical properties of ATS/ATP/HR600P = 70/9/21.

52
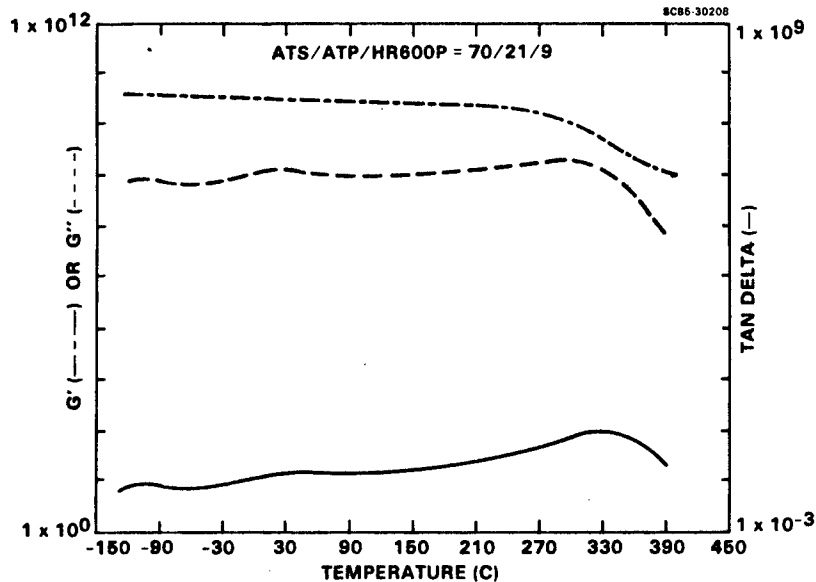
Fig. 42  Dynamic mechanical properties of ATS/ATP/HR600P = 70/21/9.

### 3.2.4  Fracture Energies of Tertiary Blends

Tertiary blends were cured in an autoclave under 100 psi at 140°C for 24 h, followed by 6 h at 177°C and a postcure of 10 h at 300°C. Fracture energies of the specimens were measured and tabulated as in Table 14. The data in Table 14 therefore indicate that the blending of ATP and HR600P indeed improved the fracture energies of ATS. However, the blended materials are still quite brittle, with a toughness below that of the epoxies.

### 3.2.5  Tensile Properties of Tertiary Blends

Tensile dog-bone specimens were fabricated by placing the blended resin in matched-die molds, degassed at 120°C, and cured in an autoclave at 140 and 177°C, respectively. However, great difficulty was encountered in obtaining either void-free or complete specimens: part of the resin charge invariably flowed out of the matched-due mold during cure, no matter how complete degassing was achieved at 120°C. Later it was found that the HR600P resin that was used

53

### Table 14

#### Fracture Energies of Tertiary Blends of ATS/ATP/HR600P

| ATS/ATP/HR600P | $(J/m^2)$ |
|---|---|
| 100/0/0 | 35.0 |
| 75/21/9 | 46.6 |
| 75/9/21 | 54.8 |
| 50/25/25 | |

belongs to an earlier version of the resin, in which the isoimide-imide conversion had not been completed. This isomerization reaction apparently continued to occur at the polymerization temperatures of 140 and 177°C with considerable outgassing, squeezing out the resin from the mold cavities. To assure ourselves that the isoimide-imide coversion was completed prior to blending, HR600P was preheated in a vacuum oven at 180°C for 10 minutes prior to incorporation into the ATS/ATP blend. The pretreatment was found to have no effect on the solubility of the resin in the tertiary blend.. (A longer heating period of 15 minutes at 180°C, however, rendered the HR600P resin insoluble in THF.) Indeed, when the tertiary blend was degassed and cured in the matched-die molds, complete devolatilization was easily obtained, without the constant bubbling previously observed with the untreated HR600P. Good quality tensile dogbone specimens were obtained.

Tensile properties of the tertiary blends were measured at room temperature, 177 and 232°C, at a crosshead rate of 0.1 mm/min. Strain was measured by foil gauges. Table 15 shows the tensile properties of tertiary blends of ATS/ATP/HR600P.

The data show that for the blend ratio of ATS/ATP/HR600P, there is a dramatic increase in the room temperature tensile strength over that of the other blend ratios. However, there is also the same dramatic decrease in tensile strength at elevated temperatures when compared to the other blend ratios. It appears that the presence of a sufficiently high ratio of either ATP or HR600P is the underlying factor in this reversal at elevated temperatures. This contrasts with the data obtained at AFWAL[18] where tensile properties of ATS/ATP blends were shown to be almost independent of compositional changes at 177°C and above.

Table 15

Tensile Properties of ATS/ATP/HR600P Blends

| ATS/ATP/HR600P | Room Temperature (MPa) | (%) | 177°C (MPa) | (%) | 232°C (MPa) | (%) |
|---|---|---|---|---|---|---|
| 70/9/21 | 64.5 | 2.0 | 50.1 | 2.9 | 43.2 | - |
| 70/21/9 | 62.0 | 1.8 | 47.1 | 2.9 | 39.4 | - |
| 50/25/25 | 76.7 | 2.5 | 38.6 | 3.2 | 26.9 | - |

# 4.0 CONCLUSIONS

## 4.1 Acetylene Terminated Polysulfones (ATS)

The evaluation of ATS resin demonstrated several of its advantages as a high temperature structural polymer. Its thermal stability and moisture sensitivity are much better than that of the state-of-the-art epoxies. The reactive end group cure mechanism is not complicated by curatives which are required in epoxies. High quality and void-free graphite fiber reinforced composites can be made by a simple "no bag" autoclave method. The low moisture sensitivity of ATS enables the fabrication of composites without the evolution of moisture which often coalesce into voids in graphite-epoxy laminates.

The program also demonstrated some of the drawbacks of the unmodified ATS resin, the most serious of which is its relatively low fracture toughness when compared to epoxies. The interlaminar shear and flexure strengths of the unidirectional laminates are not quite at par with those of the graphite/epoxies. Its lack of drap and tack also presents some difficulty in the processing and handling of the prepregs.

## 4.2 Tertiary Blends of ATS Polymer

This phase of the program was undertaken to modify the processing and brittleness of the ATS polymer, and yet retain the moisture and thermal stabilities of the resin, by blending ATS with ATP (to improve processibility) and HR600P (to improve fracture properties). The study shows that by judicious choice of the blending ratios, the tertiary blends exhibit improved processibility and fracture properties over that of the neat ATS. The thermal and rheological properties of the blends are shown to be not affected by the incorporation of ATP and HR600P.

# REFERENCES

1.  E.T. Sabourin, AFWAL-TR-80-4151 (1980).

2.  I.J. Goldfarb and W.T.K. Stevenson, AFWAL-TR-83-4011, May 1983.

3.  P.J. Dynes, AFWAL-TR-85-4053, May 1985.

4.  "Characterization of Acetylene Terminated Resin Cure States," F33615-80-C-5170, AFWAL.

5.  P. Mason, J. Chem. Phys. <u>35</u>, 1523 (1961).

6.  J. Crank, in "Diffusion in Polymers," J. Crank and G.S. Park, eds., Academic Press, N.Y., (1968).

7.  R.M. Bauer and G. Skirrow, J. Polymer Sci. <u>3</u>, 549 (1948).

8.  A. Aitken and R.M. Bauer, Trans. Faraday Soc. <u>51</u>, 116 (1955).

9.  J. Nakayama, Japan J. Appl. Phys. <u>3</u>, 422 (1964).

10. H.G. Tattersall and G. Tappin, J. Mtl. Sci. <u>1</u>, 246 (1966).

12. G.C. Sih and H. Liebowitz, in "Fracture," H. Liebowitz, ed., Vol. II, 1968, Chapter 2.

13. C.Y-C. Lee, I.J. Goldfarb, T.E. Helminiak and F.E. Arnold, Proc. 28th National SAMPE Sym. <u>699</u>, (1983).

14. C. Y-C. Lee, Polym. Mtls. Sci. and Engineering <u>51</u>, 406 (1984).

15. B.A. Reinhardt and F.E. Arnold, AFWAL-TR-80-4012.

16. P.H. Sung and C. Y-C. Lee, AFWAL-TR-83-XXXX.

17. A.V. Tobolsky and M.C. Shen, in "Advances in Chemistry Series, No. 48," American Chemical Society, (1965).

18. C.C. Kuo and C. Y-C. Lee, to be published.

APPENDIX

## HOT-MELT PREPREGGER

A single-tow pultrusion hot-melt prepregger was used to prepare prepreg of ATS resin with unsized Celion 12K graphite fiber. Three views of the prepregger are shown in Fig. A-1. The system consists of a resin reservoir and metering device mounted on the moving arm off a standard lathe. The resin reservoir is 4 in. long and 2.65 in. wide, and has a conical hole 2.5 in. in diameter at the top and 0.75 in. in diameter at the bottom. Two smooth metal rollers are staggered along the length of the reservoir. A two-part die 0.75 in. in diameter is fitted at the bottom of the reservoir. This die has an elliptically shaped hole which is 0.44 in. long by 0.10 wide at the top and tapers to approximately 0.220 in. by 0.0065 in. at the bottom.

The single graphite tow enters the resin reservoir at the top, where it is immersed in resin. The tow passes over and between the two staggered metal rollers, which tend to spread the tow and assure complete wetting by the resin. The fiber tow moves through the die which controls the amount of resin retained. The impregnated tow then passes over a smooth moving roller and onto the drum of the lathe. The lathe is set at five threads per inch which results in five tows per inch giving an area fiber weight of 174 g/m$^2$. The temperature of the resin reservoir was controlled by heating elements embedded at the four corners. The temperature was adjusted to give a resin viscosity of ~ 300 Poise.

The resin content of the prepreg was controlled mainly by the dimensions of the pultrusion die in the resin reservoir. The narrowest width tested was approximately 0.058 in. which gave a resin content of about 35.5%. At this width, the fiber tow was under considerable tension moving through the die, and any further reduction in width would result in fiber breakage.
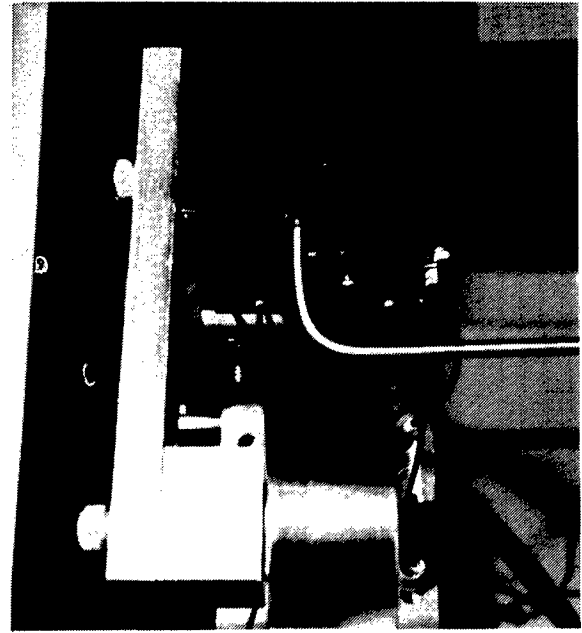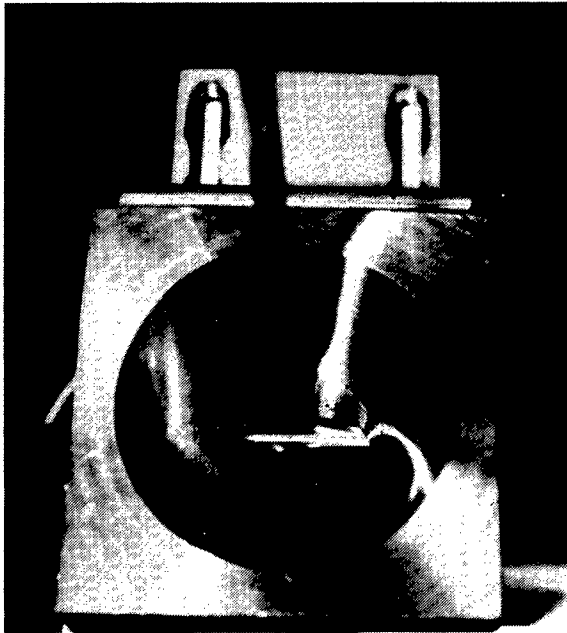
Fig. A-1.  Three views of single-tow pultrusion hot-melt prepregger.